

See discussions, stats, and author profiles for this publication at: <https://www.researchgate.net/publication/335334958>

Structural insights into the mechanism of internal aldimine formation and catalytic loop dynamics in an archaeal Group II decarboxylase

Article in *Journal of Structural Biology* · August 2019

DOI: 10.1016/j.jsb.2019.08.009

CITATIONS

4

READS

416

2 authors:



Chellam Gayathri Subash
Heptares Therapeutics

12 PUBLICATIONS 8 CITATIONS

[SEE PROFILE](#)



Narayanan Manoj
Indian Institute of Technology Madras

44 PUBLICATIONS 693 CITATIONS

[SEE PROFILE](#)

Some of the authors of this publication are also working on these related projects:



Structure Function Relationship of the PZ-ZPI complex [View project](#)



Biochemical and structural studies on a thermostable carbohydrate esterase from *Thermotoga maritima* [View project](#)

Structural insights into the mechanism of internal aldimine formation and catalytic loop dynamics in an archaeal Group II decarboxylase

Subash Chellam Gayathri¹, Narayanan Manoj^{1*}

¹Department of Biotechnology, Bhupat and Jyoti Mehta School of Biosciences, Indian Institute of Technology Madras, Chennai - 600036, INDIA.

*Corresponding Author: Narayanan Manoj (nmanoj@iitm.ac.in); Tel. (9144) 2257-4113, ORCID 0000-0002-8144-1566

Highlights

- Crystal structure of the internal aldimine form of MjDC, a PLP-dependent decarboxylase from *Methanocaldococcus jannaschii*.
- Structural evidence for water-mediated internal aldimine formation in MjDC.
- An extended hydrogen-bonding network around PLP may influence internal aldimine formation and activation.
- Structural changes associated with internal aldimine formation induces an order-to-disorder transition of the catalytic loop (CL) conformation.
- The conserved catalytic proton donor residue Tyr is expected to influence CL dynamics.

Accepted manuscript ©2019. This manuscript version is made available under the CC-BY-NC-ND 4.0 license <http://creativecommons.org/licenses/by-nc-nd/4.0/>

J Struct Biol. 2019 Nov 1;208(2):137-151. doi: [10.1016/j.jsb.2019.08.009](https://doi.org/10.1016/j.jsb.2019.08.009)

ABSTRACT

Formation of the internal aldimine (LLP) is the first regulatory step that activates pyridoxal 5'-phosphate (PLP) dependent enzymes. The process involves a nucleophilic attack on PLP by an active site Lys residue, followed by proton transfers resulting in a carbinolamine (CBA) intermediate that undergoes dehydration to form the aldimine. Despite a general understanding of the pathway, the structural basis of the mechanistic roles of specific residues in each of these steps is unclear. Here we determined the crystal structure of the LLP form (holo-form) of a Group II PLP-dependent decarboxylase from *Methanocaldococcus jannaschii* (MjDC) at 1.7 Å resolution. By comparing the crystal structure of MjDC in the LLP form with that of the pyridoxal-P (non-covalently bound aldehyde) form, we demonstrate structural evidence for a water-mediated mechanism of LLP formation. A conserved extended hydrogen-bonding network around PLP coupled to the pyridinyl nitrogen influences activation and catalysis by affecting the electronic configuration of PLP. Furthermore, the two cofactor bound forms revealed open and closed conformations of the catalytic loop (CL) in the absence of a ligand, supporting a hypothesis for a regulatory link between LLP formation and CL dynamics. The evidence suggests that activation of Group II decarboxylases involves a complex interplay of interactions between the electronic states of PLP, the active site micro-environment and CL dynamics.

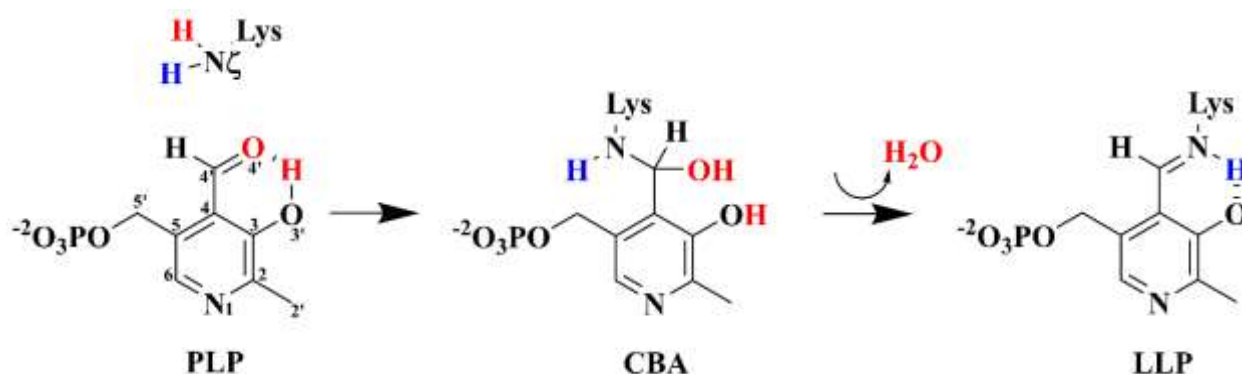
Keywords: Crystal structure; Pyridoxal phosphate; Internal aldimine formation; Decarboxylase; Catalytic loop dynamics; Extended hydrogen-bonding network

1. Introduction

Pyridoxal 5'-phosphate (PLP) is a cofactor of over 160 enzymes that catalyze different physiological reactions such as transamination, decarboxylation, racemization, deamination, among others (Percudani and Peracchi, 2003; Richard et al., 2009; Toney, 2011). Despite the plethora of reactions catalyzed by PLP-dependent enzymes, they are categorized into only 5 structural folds annotated as fold-types I–V, with each fold-type displaying functional promiscuity due to convergent evolution (Schneider et al., 2000). PLP-dependent decarboxylases catalyze the decarboxylation of diverse amino acid substrates and are involved in the biosynthesis of physiologically important amines such as catecholamines and polyamines (Bertoldi, 2014; Fenalti et al., 2007; Han et al., 2010; Kezmarsky et al., 2005; Komori et al., 2012; Kumar, 2016; Wang et al., 2014). The decarboxylases are further classified based on sequence homology into 4 groups (Group I – IV), the largest of which is the Group II decarboxylase belonging to the fold-type I superfamily (Sandmeier et al., 1994). Group II

comprises of enzymes such as 3,4-dihydroxy-phenylalanine (L-DOPA) decarboxylase (DDC), histidine decarboxylase (HDC), tyrosine decarboxylase (TyDC), tryptophan decarboxylase (WDC) and glutamate decarboxylase (GAD) that are implicated in a wide range of biological activities such as cellular homeostasis, neurotransmission, redox regulation, immune function, etc., and therefore their activities are finely regulated (Bertoldi, 2014; Burkhard et al., 2001; Capitani et al., 2003; Chen et al., 1998; Dutyshev et al., 2005; Fenalti et al., 2007; Giardina et al., 2011; Ishii et al., 1998; Kass et al., 2014; Langendorf et al., 2013; Wada et al., 1990; Zhu et al., 2016).

The first important step in PLP-dependent enzymes, including Group II decarboxylases, is the formation of a Schiff base (SB) between pyridoxal-P (the non-covalently bound form of PLP) and a conserved active site Lys residue, forming the internal aldimine (LLP). This step activates the enzyme for subsequent catalysis (Schneider et al., 2000). Upon substrate entry the internal aldimine reacts with the amino group of the substrate through a transamination reaction to form the external aldimine complex. The product of the reaction varies with the enzyme and the external aldimine complex formed (Paiardini et al., 2014; Percudani and Peracchi, 2003; Richard et al., 2009; Schneider et al., 2000; Toney, 2005; Toney, 2011). The mere binding of pyridoxal-P, its orientation, the protonation state within the active site, and the associated interactions and conformational changes in the protein are known to influence LLP formation (Dajnowicz et al., 2017a; Dajnowicz et al., 2017b; Fernandes et al., 2017; Giardina et al., 2011; Griswold and Toney, 2011; Kass et al., 2014; Langendorf et al., 2013; Malerba et al., 2007; Nishio et al., 2010; Oliveira et al., 2011; Sonnet et al., 2008; Toney, 2005; Zhu et al., 2016).



Scheme 1: Simplified mechanism for Schiff base (LLP) formation between pyridoxal 5'-phosphate (PLP) and Lys. The reaction proceeds through the formation of a carbinolamine (CBA) intermediate. Atom labels are shown for PLP and the amino group of Lys.

While mechanistic understanding of the transamination and decarboxylation steps in Group II decarboxylases is well documented, the structural factors that influence the catalytic pathway of internal aldimine formation in the enzyme environment is largely overlooked. The seemingly simple reaction involves multiple intermediate steps including a series of proton transfers, the formation of

a transient carbinolamine (CBA) intermediate, followed by loss of a water molecule to form the LLP (Scheme 1) (Ding et al., 2015; Oliveira et al., 2011; Salvà et al., 2002; Salvà et al., 2003; Sevilla et al., 1992; Snell, 1971; Sonnet et al., 2008). In fold-type I enzymes, it is known that protonation of the pyridine nitrogen (N1-PLP) atom results in the active holo-enzyme for subsequent catalysis (Griswold and Toney, 2011; Toney, 2011). Spectroscopic studies show that the formation of the CBA intermediate is a reversible process with low equilibrium constants (Chen et al., 1998; Malerba et al., 2007; Schirch and Slotter, 1966; Sevilla et al., 1992; Sonnet et al., 2008). Consequently, the structural basis of the mechanism of LLP formation in Group II decarboxylases or in other members of the fold-type I superfamily remains poorly characterized due to the limitation in obtaining *in-crystallo* snapshots of the pyridoxal-P bound form, the reaction intermediates and the LLP forms of the same enzyme. The well-described mechanism proposed using hybrid quantum mechanical (QM) calculations is that for ornithine decarboxylase (ODC), a fold-type III enzyme (Oliveira et al., 2011). In this vein, many points remain unresolved such as: (i) What are the structural determinants required to facilitate the formation and dehydration of the CBA in Group II decarboxylases? (ii) Is the activation of the cofactor driven by restructuring in the active site microenvironment? (iii) What and how large are the conformational changes associated with the transition from pyridoxal-P to LLP in these enzymes? To the best of our knowledge, the crystal structures of human DDC in the pyridoxal-P and LLP bound states represent the sole example of appropriate snapshots of the process of internal aldimine formation in a Group II decarboxylase. However, the step-wise mechanism of LLP formation was not described in the study, making it incomplete (Giardina et al., 2011).

Here we report the crystal structure of the internal aldimine form of an archaeal Group II decarboxylase from *Methanocaldococcus jannaschii* (MjDC), determined at 1.72 Å resolution. The crystal structure of MjDC in the pyridoxal-P bound form is available in the PDB (PDB ID: 3F9T, Joint Centre for Structural Genomics, unpublished). Using the two structures and a model of the CBA intermediate in combination with biochemical data from substitution mutants, we could identify specific residues, water molecules and an extended hydrogen-bonding network that are likely to play key mechanistic roles along the pathway to LLP formation. Furthermore, analyses of structural rearrangements revealed the coupling of the dynamics of the catalytic loop (CL) to LLP formation, suggesting an additional regulatory role for the CL in Group II decarboxylases.

2. Materials and methods

2.1 Site-directed mutagenesis and protein expression. The plasmid containing *MjDC* gene in pSpeedET vector, encoding residues 1-397 was purchased from *DNASU* (JCSG 390948; PSI:

Biology Materials Repository Clone ID: MjCD00289364, <http://psimr.asu.edu/>.) (Seiler et al., 2014). The clone contained an N-terminal 6-His Tag (MGSDKIHHHHHHENLYFQG), cleavable by Tobacco Etch Virus protease. The M37F, H132A, S134A, F133V, F133S, Y273F, Y273W, T181V and V269A variants of MjDC were constructed using Phusion polymerase (*New England Biolabs*) as per manufacturer's protocol. The oligonucleotides used for mutagenesis are listed in table S2. All mutations were confirmed by DNA sequencing.

Wild type (WT) (Uniprot Id Q60358) and mutant MjDCs were transformed into BL21-CodonPlus (DE3)-RIL cells (*Agilent Technologies*). Cells were grown at 37 °C, in LB media containing kanamycin (50 µg ml⁻¹) and chloramphenicol (34 µg ml⁻¹). The cultures grown at 37 °C were induced at an OD₆₀₀ of 1.0 with 0.5 mM IPTG and harvested 4 hours post induction by centrifugation at 4500×g for 10 min. The cells were resuspended in lysis buffer (20 mM HEPES pH 8.0, 200 mM NaCl, 2 mM DTT and 0.1 mM PMSF) and incubated at room temperature (RT) for 30 min. The cells were lysed by sonication using a VC 500 Sonic Vibra-cell (Sonics Materials, Inc.) with an amplitude setting of 27% and a pulse of 2 s 'ON' followed by 4 s 'OFF'. Cell debris was clarified by centrifugation at 18,514×g for 1 hour at 4 °C to separate the soluble and insoluble fraction. The soluble fraction was subjected to thermal precipitation at 80 °C for 20 min and centrifuged at 18,514×g for 30 min. The supernatant was loaded on a gravity flow Ni-Nitrolotri-acetic acid (Ni²⁺-NTA) agarose column (GE Healthcare, UK) equilibrated with buffer A (20 mM HEPES pH 8.0, 200 mM NaCl, 10 mM imidazole) at RT. The column was washed with 20 column volumes of buffer A and 20 column volumes of buffer B (20 mM HEPES pH 8.0, 200 mM NaCl, and 30 mM imidazole). The protein was eluted using buffer C (20 mM HEPES pH 8.0, 200 mM NaCl, and 150 mM imidazole). The eluted protein was subjected to a second purification step by size exclusion chromatography using a HiLoad 16/60 Superdex 200 pg column (GE Healthcare, UK). The protein was finally concentrated to 40 mg/ml in storage buffer (20mM HEPES pH 8.0, 20mM NaCl and 5 mM DTT) and stored at -80 °C. The Y273 variants were purified in buffers containing TRIS instead of HEPES, since, they tend to aggregate in the latter. Protein concentration was estimated by UV absorption at 280 nm using a molar extinction coefficient of 34310 M⁻¹ cm⁻¹ for the WT and all other mutants except the Y273 variants. The molar extinction coefficients used for Y273F and Y273W were 32820 M⁻¹ cm⁻¹ and 38320 M⁻¹ cm⁻¹, respectively.

The oligomeric status of MjDC was determined using a Superdex 200 10/300 GL analytical column on an AKTA FPLC system (GE Healthcare, UK), maintained at 4°C. The column was equilibrated with 100 mM HEPES buffer, pH 8.0. The protein (2.0 mg/ml) was loaded onto the column and eluted at a flow rate of 0.4 ml/min. The apparent molecular weight of the eluting species

was determined by comparing their elution volume to that of a set of molecular weight standards under the same experimental conditions (Fig S1).

2.2 Enzyme assays. Decarboxylase assay was performed as described by previously with some modifications (Kezmarsky et al., 2005; Phan et al., 1983). Briefly, 10 μg of enzyme was incubated for 5 min with 0.5 mM L-tyrosine and 20 μM PLP in 50 mM HEPES, pH 8.0, at 80°C (final volume 250 μl). The reaction was stopped by adding equal volume of 1M K_2CO_3 . Equal volume of 2,4,6-trinitrobenzenesulfonic acid (TNBS) (to a final concentration of 10.2 mM) and a 2-fold excess of toluene were added to the reaction mixture and incubated at 42 °C for 1 h with continuous mixing. The concentration of the trinitrophenyltyramine derivative in the toluene layer was measured at 340 nm with a SpectraMax multimode microplate reader (*Molecular Devices, USA*) and calculated using tyramine standards. To identify optimum temperature of the enzyme activity, purified MjDC was incubated at different temperatures from 20 °C to 99 °C for ten minutes and then assayed for specific activity using the assay conditions. The effect of pH was tested in a three-component buffer system, comprising of citrate, HEPES and TRIS buffers, in the pH range of 4.0 – 9.0 under standard assay conditions. Each experiment was performed in triplicates. Figures were made using GraphPad Prism 5.0 software.

2.3 Spectral measurements. Absorption measurements with recombinant WT and mutant enzymes, to detect the presence of the cofactor and internal aldimine formation, were made with a Jasco V-550 spectrophotometer using 20 μM protein in 50 mM HEPES buffer, pH 8.0, 100 μM DTT at 25 °C, unless specified otherwise. Temperature was controlled during the measurements with a Peltier temperature controller attached to the spectrophotometer. Appropriate buffer spectra were recorded and subtracted from the protein spectra. PLP content was estimated by UV-vis absorption at 387 nm by releasing the bound PLP into 0.1 M NaOH and using 6600 $\text{M}^{-1} \text{cm}^{-1}$ as the molar extinction coefficient of PLP.

2.4 Sequence and structural alignment of Group II decarboxylases. The sequences of homologous archaeal, bacterial and eukaryotic decarboxylases were aligned based on structural superposition using WT MjDC as the template. The sequence alignment was generated using a structure-based superposition program, Dali Lite v.3 and manually inspected. Sequence alignment figure was generated using ESPRIPT 3.0 (<http://espript.ibcp.fr/ESPrIPT/cgi-bin/ESPrIPT.cgi>) (Robert and Gouet, 2014). Amino acid decarboxylase sequences were retrieved from UniProt database:

M.jannaschii_MjDC: WT *Methanocaldococcus jannaschii* tyrosine/aspartate decarboxylase; *S.thermophilus_StDC*: *Sphaerobacter thermophilus* dsm 20745 PLP dependent decarboxylase, (PDB ID: 4RIT); *H.sapiens_GAD65*: *Homo sapiens* glutamate amino acid decarboxylase isoform 2 (PDB ID: 2OKK); *S.scrofa_DDC*: *Sus scrofa* L-DOPA decarboxylase (PDB ID: 1JS3); *R.gnavus_WDC*: *Ruminococcus gnavus* tryptophan decarboxylase (PDB ID: 4OBU); For the comparison of the closed CL the following structures were used. *M.jannaschii_MjDC*: *M. jannaschii* tyrosine/aspartate decarboxylase aldehyde form (PDB ID: 3F9T); *H. sapiens_GAD67*: *Homo sapiens* glutamate amino acid decarboxylase isoform 1 in complex with γ -amino butyric acid (PDB ID: 2OKJ); *H.sapiens_HDC*: *Homo sapiens* histidine decarboxylase in complex with histidine methyl ester (PDB ID: 4E1O); *R.gnavus_WDC*: *Ruminococcus gnavus* tryptophan decarboxylase in complex with (S)- α -fluoromethyltryptophan (PDB ID: 4OBV).

2.5 Crystallization, data collection and processing. Crystals were grown by hanging-drop vapor diffusion method at 20 °C. The volume of the reservoir solution was 500 μ l and the drop volume were 2 μ l, containing 1 μ l of protein sample and 1 μ l of reservoir solution. The reservoir solution contained 0.1 M sodium citrate pH 5.4, 0.2 M sodium potassium tartrate, 2.0 M ammonium sulphate. 2.0 M ammonium sulphate and 40 % glycerol were used as the cryo-protectant before flash freezing. Crystals grew in a span of 10–15 days using protein concentration of ~20 mg/ml. X-ray diffraction data of holoMjDC•LLP were collected from a single crystal under cryo conditions (100 K nitrogen stream) at the BM14 beamline (European Synchrotron Radiation Facility, Grenoble, wavelength 0.91841 Å). The collected data was indexed and integrated with *iMOSFLM* and scaled using *SCALA* (Battye et al., 2011; Evans, 2011; Winn et al., 2011). The data was indexed in the tetragonal space group P4₃2₁2 with cell parameters a=b=98.39 Å, c=121 Å; $\alpha=\beta=\gamma=90^\circ$ and processed to a resolution of 1.72 Å. Data collection statistics are given in Table 1.

2.6 Structure determination, model building and refinement. The structure was solved by molecular replacement with *MOLREP* (Lebedev et al., 2008) program using a single subunit of apoMjDC•PLP_{ALD} (PDB ID: 3F9T) as the search model. One subunit was identified in the asymmetric unit of the unit cell. Restrained refinement was performed using iterative rounds of *REFMAC* (Murshudov et al., 1997) and *PHENIX* (Adams et al., 2011). Visual inspection in *COOT* was done to improve individual B factor refinements with manual water deletion and incorporation. Refinement protocols also included simulated annealing refinement to remove model bias. Five per cent of the reflections were selected randomly for calculating R_{free} for cross validation. Quality of

the models were verified and validated using the *COOT* package and *MOLPROBITY* (Chen et al., 2010; Emsley and Cowtan, 2004). Final refinement statistics are as shown in Table 1. Figures were made using PyMol (The PyMOL Molecular Graphics System, Version 2.0 Schrödinger, LLC).

The experimental omit maps were generated after molecular replacement, rigid body and restrained refinements using simulated annealing at 5000 K with appropriate models lacking the atoms of PLP, the side chain of Lys245, LLP and the residues 267-280, in *PHENIX* (Adams et al., 2011). An *ab initio* model of the missing 4 residues of the CL was built as follows. First, we reconstituted the missing loop in each monomer using the Modeller 9.11 module in *UCSF Chimera* (Pettersen et al., 2004). The structure with the lowest DOPE score and the highest GA341 assessment score was chosen and was subjected to 500 steps of energy minimization using the geometry minimization module in *PHENIX* with the remaining residues restrained (Adams et al., 2011). The CBA intermediate was built using the *JLigand* module in *CCP4* suite by modifying the structure of the LLP/PMP complex present in the active sites of StDC (PDB ID: 4RIZ chain C) (Winn et al., 2011). The coordinates of the CBA intermediate were superposed over the coordinates of ligands in the active site of StDC to yield the CBA intermediate bound structure.

2.7 Accession Codes. Coordinates and structure factors have been deposited in the Protein Data Bank under the accession number 6JY1.

3. Results and Discussion

3.1 Protein expression, purification, oligomeric state and biochemical characterization. MjDC is a promiscuous enzyme that catalyzes the decarboxylation of L-tyrosine and L-aspartate to tyramine (EC 4.1.1.25) and β -alanine (EC 4.1.1.11), respectively (Kezmarsky et al., 2005; Wang et al., 2014). Recombinant MjDC protein was overexpressed in *E. coli* BL21-CodonPlus (DE3)-RIL cells and was purified to homogeneity (Fig. S1A). The protein is composed of 396 residues and exists as a dimer in solution as indicated by size-exclusion chromatography (Fig. S1B). MjDC showed the expected absorbance maxima at 330 nm (enolamine) and 418 nm (ketoenamine) corresponding to the different tautomeric forms of the internal aldimine (Fig. S1D). The estimated stoichiometry of 2 molecules of bound PLP is consistent with the dimeric state of MjDC. It is to be noted that the absorption spectra measurements reported here are only indicative of formation of the internal aldimine and does not provide an estimate of the formative constants. L-tyrosine was used as the substrate to characterize the activity of the recombinant WT and mutant proteins. Decarboxylase assay was measured by monitoring the production of trinitrophenyltyramine derivative as described

earlier (Phan et al., 1983). The WT showed maximum activity at 90 °C (Fig. S1E) and pH 8.0 (Fig. S1F) consistent with an earlier report (Kezmarsky et al., 2005).

3.2 Overall structure of *holoMjDC•LLP*. The crystal structure of recombinant WT MjDC bound to pyridoxal-P (hereafter referred to as apoMjDC•PLP_{ALD}) in the orthorhombic space group P2₁2₁2 determined at 2.11 Å resolution is available in the PDB (PDB ID: 3F9T). Using a different crystallization condition, we obtained crystals of MjDC in a tetragonal space group (P4₃2₁2) with one subunit in the asymmetric unit. The structure was solved by molecular replacement using a single subunit of apoMjDC•PLP_{ALD} and refined to a resolution of 1.72 Å. Clear electron density was visible for 390 residues that encode the protein. The terminal residues and 4 residues (275–278) that are part of the “flexible” CL were disordered and not modelled in the structure (Fig. 1). Interestingly, continuous electron density was observed between PLP and the active site Lys245 residue suggesting SB formation between the C4' atom of pyridoxal-P and the N ζ atom of Lys245. This is as expected for the presence of an internal aldimine in the holo-enzyme (Fig. 2A). We refer to this form of MjDC as *holoMjDC•LLP*. The expected physiologically relevant homodimeric state of *holoMjDC•LLP* is formed by two subunits related by a crystallographic 2-fold axis and is identical to that observed in the dimer present in the asymmetric unit of the apoMjDC•PLP_{ALD} crystal form (Fig. S2A).

The *holoMjDC•LLP* subunit contains the characteristic architecture of the fold-type I superfamily comprising of three domains, a PLP-binding large domain (residues 30-302), a small C-terminal domain (CTD, residues 303-395) and a N-terminal domain (NTD, residues 1-30) (Fig. 1C and S2) (Schneider et al., 2000). The large domain comprises of a seven stranded β sheet stacked by five α helices, folding into a typical $\alpha/\beta/\alpha$ sandwich (Fig 1A). The strand order of the β sheet is β (1-7-6-5-4-2-3), with β 7 antiparallel to the otherwise parallel sheet. The active site Lys245 residue is present on a loop connecting strands β 6 and β 7. The CTD comprises of two β strands with strand order β (8-9), flanked by three α helices on one side (Fig. S3). The large domain is connected to the small domain *via* an extended α helix that forms a tight perpendicular bend at a conserved Gly302 residue (Fig. S4). This bend positions C-terminal residues between strands β 9 and β 10 near the active site pocket (Fig. S3). The NTD of the protein is exclusively α helical (Fig. S3). This domain forms a domain swap with the adjacent subunit resulting in a clamp-like structure to form a part of the dimeric interface, typical of homodimeric Group II decarboxylases (Fig. S2 and S5A) (Fenalti et al., 2007; Giardina et al., 2011; Komori et al., 2012).

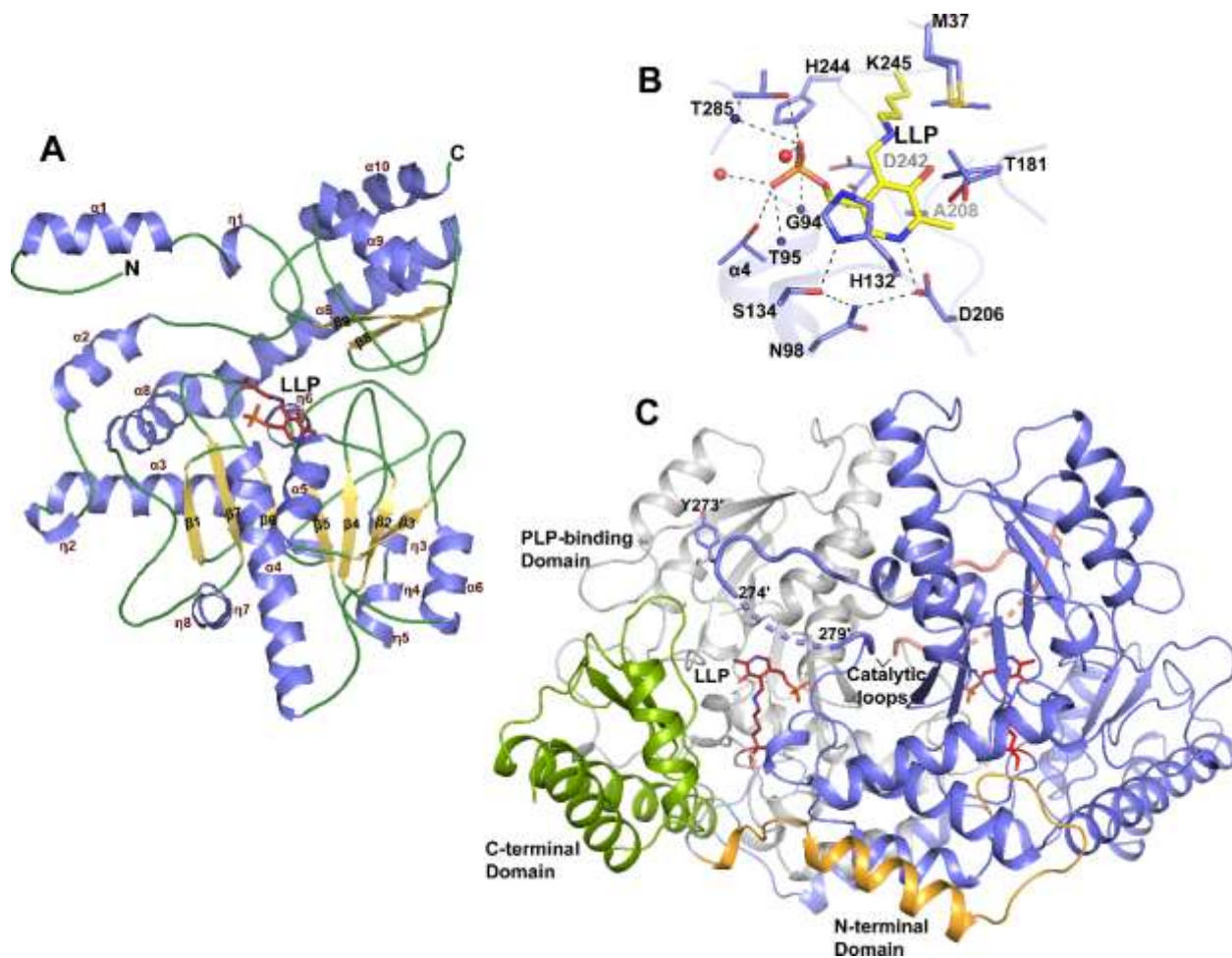


Figure 1: Structure of holoMjDC•LLP. (A) Ribbon representation of a subunit of MjDC depicting its overall fold. Helices are colored blue, strands are in yellow and loops are green. LLP is shown in red stick representation. Secondary structure elements are labelled numerically. (B) Close up view of the PLP binding pocket. Cofactor binding residues are shown in stick representations (blue sticks). The catalytic Lys245 has formed a Schiff base with PLP (LLP) and is shown in yellow. Waters are shown as red spheres, and backbone amides of Thr95 and Gly94 are shown as blue spheres. Hydrogen bond interactions ($< 3.2 \text{ \AA}$) of the cofactor with the residues lining the active site pocket are displayed as dashed black lines. (C) Ribbon diagram of the MjDC dimer. The domain organization of one subunit is highlighted using different colors (PLP binding domain is shown in grey, C-terminal domain in green and N-terminal domain in orange, the catalytic loop is shown in pink) while the other subunit is shown in blue. Note the domain swap of the NTD with the adjacent monomer. LLP and the catalytic tyrosine are shown as red and blue sticks respectively. Dashes between residues 274 and 279 indicate the missing catalytic loop segments.

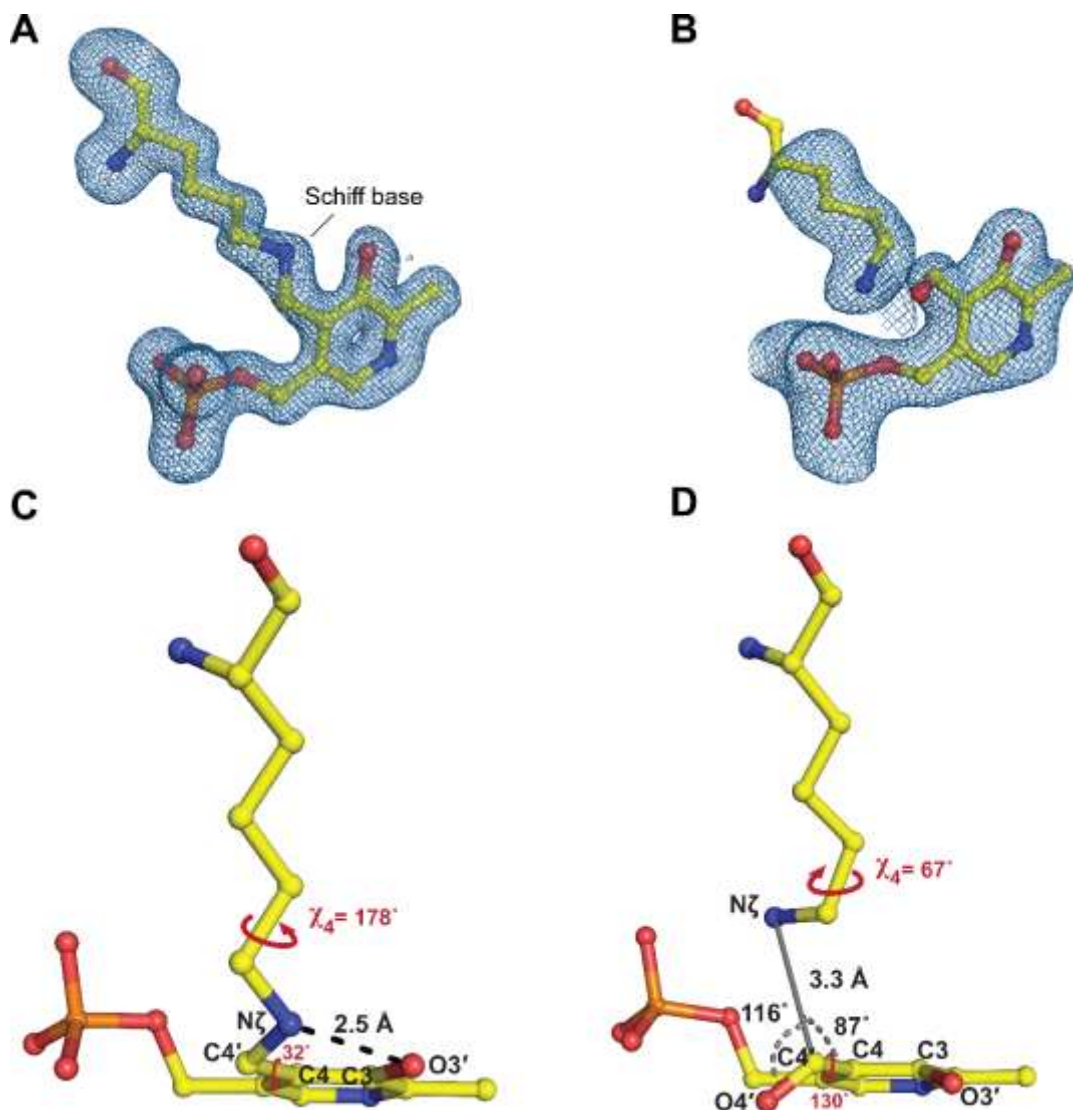


Figure 2: Structures of PLP in the active site of holoMjDC•LLP and apoMjDC•PLP_{ALD}. Fo–Fc omit maps as found in the active sites of (A) holoMjDC•LLP (contoured at 3.4 σ) and (B) chain B of apoMjDC•PLP_{ALD} (contoured at 2.5 σ) are shown as blue mesh representation. The density corresponds to a simulated annealing omit map (5000 K) calculated from a model lacking the atoms of LLP (for holoMjDC•LLP), PLP and the side chain of Lys245 (apoMjDC•PLP_{ALD}). LLP, Lys245 and PLP are shown as yellow sticks, superposed over the maps. Schiff base (SB) linkage is indicated. Panels (C) and (D) show the geometry of PLP and Lys245 after and before SB formation, respectively. Torsion angles are shown as red arrows and labels. An imaginary axis passing through N ζ and C4' atoms is shown as a grey bold line with the corresponding angles formed with that axis shown as grey dashed arcs. Hydrogen bond interaction is displayed as a dashed black line.

A DALI search of the PDB using the tertiary structure of MjDC revealed significant structural similarity with other Group II decarboxylases (Holm and Laakso, 2016). These include TyDCs (PDB IDs: 5HSJ (Zhu et al., 2016), 6EEM unpublished); DDCs (PDB ID: 1JS3 (Burkhard et al.,

2001), 3RCH (Giardina et al., 2011), 3K40 (Han et al., 2010)); HDCs (PDB ID: 4E1O (Komori et al., 2012)); WDCs (PDB ID: 4OBV (Williams et al., 2014), 6EEW unpublished); GADs (PDB IDs: 2OKJ (Fenalti et al., 2007; Kass et al., 2014; Langendorf et al., 2013), 2OKK (Fenalti et al., 2007; Kass et al., 2014; Langendorf et al., 2013), 3VP6 (Kass et al., 2014; Langendorf et al., 2013), 6ENZ (Raasakka et al., 2018), 3HBX (Gut et al., 2009), 5GP4 (Huang et al., 2018), 3FZ6 (unpublished), 1PMO (Capitani et al., 2003; Gut et al., 2006), 2DGK (Gut et al., 2006), 1XEY (Dutyshev et al., 2005)); a decarboxylase of unknown function from *Sphaerobacter* (PDB ID: 4RIT, unpublished) and cysteine sulfinic acid decarboxylase (PDB ID: 2JIS, unpublished). The homologs share a Z-score in the range 29.8–63.4 and root mean square deviation (rmsd) of 0.8–3.2 Å, aligned over 359–379 C α atoms. The pairwise sequence identities based on the structural alignment are in the range 16–25 %, indicating significant divergence at the level of sequence. Superposition of these structures revealed that the core of the large domain and the CTD are largely structurally conserved with moderate changes in the lengths and orientations of the secondary structural elements (Fig. S6).

The most striking structural difference between MjDC and the homologs occur in the NTD. In animal homologs, the NTD is comprised of three helices (α 1N, α 2N, α 3N). The α 1N helix along with α 1L helix from the large domain forms a four-helix bundle with the corresponding regions in the opposite subunit (Fig. S5B). In human DDC and human GADs, this bundle acts as a hinge that assists the opening up of the dimer *via* a rigid body rearrangement, in the absence of the cofactor (Giardina et al., 2011; Kass et al., 2014). In hexameric bacterial decarboxylases, a long loop precedes an NTD helix and together contributes to both the dimer and hexamer interfaces. In this case, the loop region undergoes changes in conformation in response to changes in pH, affecting its cellular localization and function (Capitani et al., 2003; Gut et al., 2006). The NTD of MjDC is shorter, containing only one helix (α 1N, equivalent to the α 3N of DDC), although the overall organization of the dimers and the corresponding interfaces are similar between MjDC and other homodimeric Group II decarboxylases. Interestingly, the NTD architecture of MjDC resembles that of a functionally distinct PLP-dependent enzyme, dimeric sphingosine-1-phosphate lyase (SPL) from *Burkholderia pseudomallei* (Fig. S5C). Indeed, this enzyme is the closest structural homolog in the DALI search (PDB ID: 5K1R), with a Z-score of 43.2, sequence identity of 25 %, rmsd of 2.3 Å over 379 C α pairs and also shares the same dimeric arrangement (Bourquin et al., 2010; McLean et al., 2017). Together, it appears that the NTD of Group II decarboxylases have evolved divergent architectures to suit different regulatory functions *via* modulation of inter-subunit interfaces (Giardina et al., 2011; Kack et al., 1999; Schneider et al., 2000).

The active site of MjDC is located in a deep cleft at the dimer interface of the large domains (Fig. 1C and S2). In the apoMjDC•PLP_{ALD} dimer, the flexible CL comprising of residues 268-280 that hosts the conserved catalytic Tyr273 assumes a “closed” state conformation that sequesters the active site from the solvent (Fig. 3C and S2C). The CL undergoes a large conformational change between apoMjDC•PLP_{ALD} and holoMjDC•LLP structures (rmsd ~7.3 Å for C α atoms of residues 268-274) (Fig. 3A). As a consequence, in holoMjDC•LLP, the conformation of the CL renders the active site “open” to the solvent resulting in the formation of a pocket with a mouth-opening of ~15 Å (Fig. 3D and S2B).

The tertiary and quaternary structures are otherwise completely conserved between the two (rmsd ~0.33 Å over 384 C α atoms) (Fig. S2). In general, in Group II homodimeric decarboxylases, the CL is longer by 6–11 residues compared to that in MjDC (Fig. 3B and S7B). Furthermore, the CL regions are largely disordered in the internal aldimine forms whereas in the external aldimine form, including human HDC (in complex with histidine methyl ester, PDB ID: 4E1O), human GAD67 (in complex with γ -amino butyric acid, PDB ID: 2OKJ) and bacterial tryptophan decarboxylase (in complex with [5-hydroxy-4-[(1E)-4-(1H-indol-3-yl)-3-oxobut-1-en-1-yl]-6-methyl-pyridin-3-yl]methyl-dihydrogen-phosphate, PDB ID: 4OBV), the CL is an ordered segment that shields the active site cavity (Fenalti et al., 2007; Komori et al., 2012; Williams et al., 2014). Remarkably, the conformation of the closed CL in apoMjDC•PLP_{ALD} is similar to that observed in the external aldimine forms of the homologs (Fig. S7B).

Within the active site of holoMjDC•LLP, Lys245 anchors PLP as a SB through its N ζ atom (Fig. 1B). The pyridine ring of PLP is completely buried within the active site by multiple interactions with conserved residues such as parallel π -stacking with His132 and a hydrophobic interaction with the methyl group of Ala208. The N1-PLP forms a hydrogen bond with Asp206 as observed for other members of this superfamily (Bertoldi, 2014; Casasnovas et al., 2012; Caulkins et al., 2014; Limbach et al., 2011; Toney, 2011). An extended hydrogen-bonding network involving His132, Ser134, Asn98 and Asp206 connects the buried pyridine N1 to the bulk solvent. Three residues, Thr181, Met37 and Asp242, around the cofactor binding pocket display dual conformations. Interactions with the cofactor from the trans-subunit is observed only at the ‘phosphate group binding cup’ (Denesyuk et al., 2003). The negative charge on the phosphate group is further stabilized by the N-terminal dipole of helix α 4 of the cis-subunit.

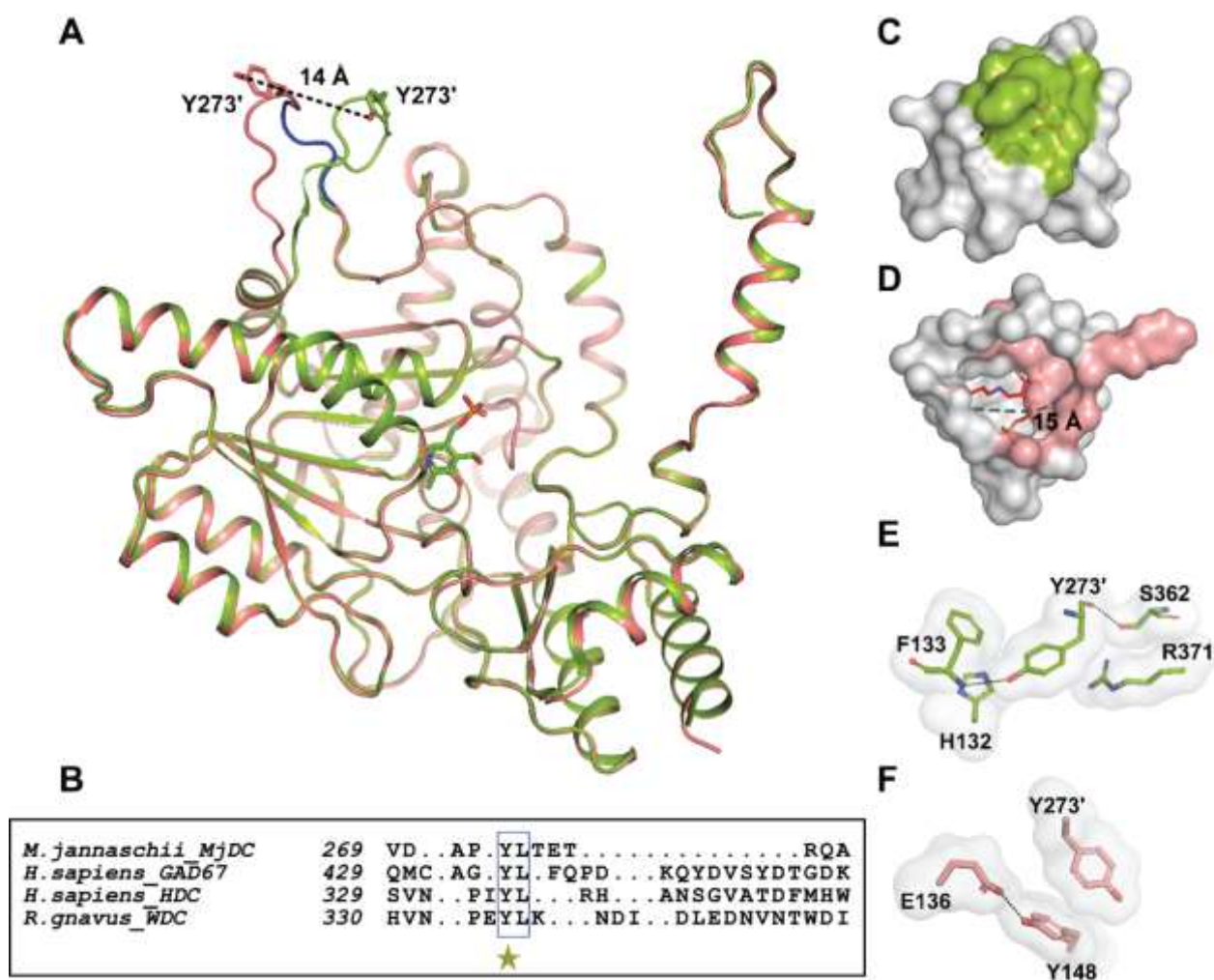


Figure 3: Structural dynamics of the catalytic loop (CL) in MjDC. (A) Cartoon representation of the structural superposition of a single subunit of apoMjDC•PLP_{ALD} (green) and holoMjDC•LLP (pink) showing the open and closed conformations of the flexible CL comprising residues 268-280. The catalytic Tyr273' and PLP are shown in stick representation. The *ab initio* model of the CL (residues 275-278) is colored in blue. (B) Structure based sequence alignment of the ordered CL regions of ligand bound, mutant or aldehyde forms of decarboxylases. This aligns the catalytically active tyrosine across all the structures. Panels (C) and (D) show surface representations of the active site cavity of the closed and the open states, respectively, in the same orientation. The closed CL is shown in green and the open CL is shown in pink. PLP, Lys245 and LLP are shown as red sticks. Panels (D) and (E) show surface representations of the stacking interactions made by Tyr273' with the adjacent subunit. The interactions made by the catalytic Tyr273' in the closed state is shown as green sticks and the open state is shown as pink sticks.

3.3 Role of enzyme active site in the formation of the internal aldimine. In general, the mechanism of LLP formation has been indirectly inferred from spectroscopic techniques and computational studies using model reactions (Chen et al., 1998; Malerba et al., 2007; Sonnet et al., 2008). The structural basis of the mechanism in an enzyme environment was most recently examined in detail

for ODC, a structurally well-characterized fold-type III PLP-dependent enzyme. This computational study using density functional theory (DFT) calculations showed that given the appropriate geometry of the pyridoxal-P and Lys reactants, the nucleophilic attack occurs spontaneously, whereas a conserved Cys360 residue is required to form the carbinolamine intermediate. Although rate limiting, the dehydration step is a straightforward process wherein formation and release of a water molecule is accomplished when a proton transfers from the phenol to the hydroxyl group of the carbinolamine intermediate resulting in the formation of the internal aldimine (Salvà et al., 2003; Oliveira et al., 2011). The different folds and active site architectures between the fold-type I and III superfamilies suggest that the structural basis for this mechanism is likely different for each fold-type or for even individual members across families. For instance, the residue structurally equivalent to that of Cys360 in ODC is absent in the fold-type I enzymes. The structure of apoMjDC•PLP_{ALD} contains pyridoxal-P bound in the active site (Fig. 2B). This is a rather unusual feature (observed in only 36 out of 801 structures of fold-type I homologs in the PDB) since PLP is usually present as SB or gem-diamines (Bertoldi, 2014; Paiardini et al., 2014; Toney, 2005). It appears that crystallization conditions favored the fortuitous formation of apoMjDC•PLP_{ALD}. The availability of the structures of reactant apoMjDC•PLP_{ALD} and product holoMjDC•LLP states provided a unique opportunity to elucidate enzyme features and propose a plausible structural basis of LLP formation, consistent with previous theoretically proposed structures of reactants and reaction intermediates (Oliveira et al., 2011; Salvà et al., 2003; Sonnet et al., 2008) (Scheme S1).

3.3.1 Interactions of pyridoxal-P in apoMjDC•PLP_{ALD}. The pyridoxal-P enzyme interactions in apoMjDC•PLP_{ALD} show minor differences between the two independent subunits in the asymmetric unit. Since the difference Fourier (Fo-Fc) map of pyridoxal-P in chain B appeared better ordered than that in chain A, chain B was chosen to carry out the comparative analysis throughout this study. In the geometry of apoMjDC•PLP_{ALD} interactions, the N ζ of the catalytic Lys245 residue is at a distance of 3.3 Å from the C4', while the orientation of the amine is in a gauche (-) conformation positioned in a plane perpendicular to that of the pyridoxal ring (N ζ -C4'-C4 angle of 87°, N ζ -C4'-O4' angle of 116°), optimal for nucleophilic attack of N ζ on C4' (Fig. 2D). The conformation of Lys245 is maintained by two ionic interactions of the N ζ atom with OP4 (3.0 Å) atom of the PLP phosphate group and with the O δ 2 atom of Asp242 (2.5 Å) (Fig. 4 and 5A). Further, the O4'-C4'-C4-C3 angle is -130° with the O4' oriented away from the phenol group O3' (3.7 Å) (Fig. 2D and 4). This conformation of the O4' is stabilized by two hydrogen bonds, namely, a water bridged hydrogen bond (2.7 Å from W1_{MJ}) with the N ϵ 2 atom of a conserved His132 residue and another directly with

the N ϵ 2 atom of His132 (2.8 Å) (Fig. 4 and 5A). The geometry of pyridoxal-P thus corresponds to the inactive state of the enzyme.

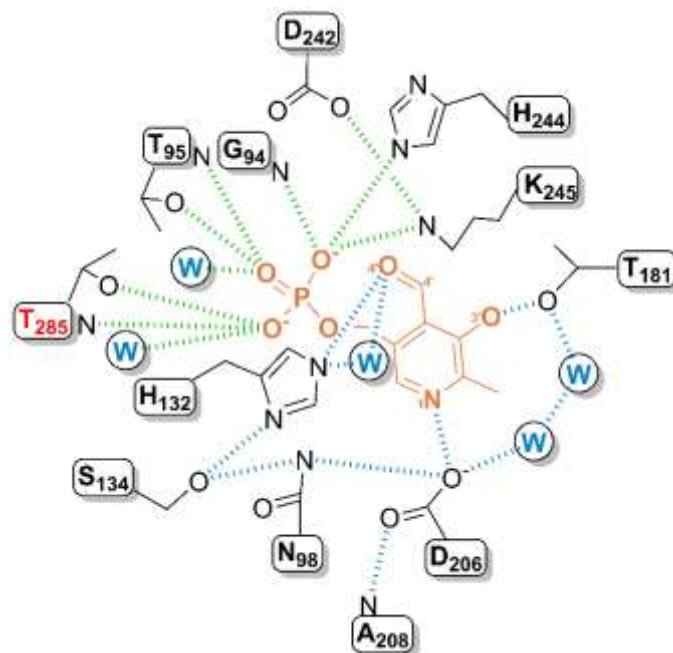


Figure 4: Schematic depiction of hydrogen bond interactions (< 3.2 Å, dashed lines) of the cofactor with residues and structural water molecules (shown in blue) in the active site of apoMjDC•PLP_{ALD}. Pyridoxal-P is colored in orange. The extended hydrogen-bonding network interactions are shown in blue. All other interactions with the cofactor are shown in green. T285 from the adjacent subunit is shown in red. The atom numbers of the phenol O3', the aldehyde O4', the nucleophilic C4' and the N1-PLP are shown.

3.3.2 Nucleophilic attack of Lys245 on pyridoxal-P. In the first step, a geometric reorientation of the O4' towards the O3' will result in the formation of an intra-molecular shared hydrogen bond between the phenol (O3') and the aldehyde (O4') groups of PLP. This will result in an extended delocalized π system with the pyridine ring thereby enhancing the electrophilic character of the C4'. Next, for the nucleophilic attack, it is necessary for Lys245 to first break the ionic interaction with phosphate. This enables a conformational rearrangement of the N ζ atom to allow a closer contact with C4', while maintaining the characteristic angle (N ζ -C4'-O4' angle of $105^\circ \pm 5^\circ$), suggested by Burgi and Dunitz for this type of reaction (Burgi et al., 1974). Following this, N ζ is covalently linked to C4' resulting in its sp^3 hybridization with accumulation of positive charge at the N ζ atom (Scheme S1). This positive charge is expected to be stabilized by its interaction with Asp242 (Fig. 5A). During the nucleophilic attack, complete transfer of the proton to the aldehyde group O4' results in a phenoxide ion at the O3' (Scheme 2A) (Sonnet et al., 2008). The side chain of a conserved Thr181 residue within 2.8 Å from the O3' in apoMjDC•PLP_{ALD} is expected to play the charge stabilization role here (Fig. 5A).

3.3.3 Formation of the carbinolamine intermediate. The next step in the reaction is the formation of the CBA intermediate. The formation of this intermediate in the fold-type I transaminases was proposed by Metzler in 1985 (Metzler and Christen, 1985). Spectroscopic evidence from *E.coli* serine hydroxyl methyl transferase (SHMT) and GADB are suggestive of the occurrence of this intermediate (Malerba et al., 2007; Pennacchietti et al., 2009). During CBA formation, a proton transfers from the N ζ to the O4' resulting in two hydroxyl groups, one each at O4' and O3', respectively (Scheme 2B) (Salvà et al., 2003). The structure of the CBA intermediate has been described earlier in fold-type III enzymes and would most likely resemble the 'PXP' ligand (Fig. 5B) present in the crystal structure of ODC (PDB ID: 1SZR) (Jackson et al., 2004). In this geometry of the PXP intermediate, the C4' atom is clearly present in a tetrahedral sp^3 -like configuration. The hybridization of the N ζ changes from sp^3 to sp^2 and the O4' and O3' are within hydrogen bonding distance of each other (Salvà et al., 2002).

To the best of our knowledge, the sole report of a crystal structure of a CBA intermediate in fold-type I enzymes is that formed in the PLP substrate complex prior to external aldimine formation in chicken aspartate aminotransferase (AAT, PDB ID: 1IVR) (von Stosch, 1996). However, the structure of the CBA intermediate, prior to internal aldimine formation has not been reported yet and hence the enzyme environment required for this step is unclear. In this context, we screened the PDB for homologous enzymes bound to ligands that resemble the CBA intermediate of the internal aldimine step of the reaction. We identified five high resolution (1.8–2.2 Å) crystal structures of WT (PDB ID: 4RLG, 4RIT) and mutants (PDB ID: 4RIZ, 4RJ0 and 4RM1, Midwest Center for Structural Genomics, unpublished) of the Group II decarboxylase from *Sphaerobacter thermophilus* (StDC) that enabled us to model a hypothetical structure of the CBA. Each of the three mutant structures and one WT structure (PDB ID: 4RLG) have four independent subunits in the crystallographic asymmetric unit. Among these, four active sites of the WT, and six active sites of the mutants (PDB: 4RM1, chains C and D; 4RIZ, chains A, C and; 4RJ0, chain D) contain a mixture of two discrete ligands, modelled as LLP and pyridoxamine 5'-phosphate (PMP), respectively (Fig. 5C). Interestingly, the ligand geometries when taken together resemble that of the CBA intermediate wherein the N4' of PMP occupies the position equivalent to that of the O4' of CBA. Moreover, examination of the electron density around the C4' atom indicates a sp^3 -like geometry, consistent with that expected in the CBA moiety. Taking these structures into consideration we generated the model of a carbinolamine intermediate in the active site of StDC. The anticipated geometry of the enzyme-CBA interactions will resemble the model with the N ζ atom maintaining a sp^3 like configuration (Fig. 5D). The phenoxide at O3' is stabilized by the interaction

with the O_γ of Thr247 (Thr181 in MjDC) (3.0 Å). The distance between the O3' and O4' is 2.8 Å indicating that the intra-molecular hydrogen bond is probably retained between the two atoms. The O4' atom also makes a hydrogen bond to water W1_{ST} (2.7 Å) (Fig. 5D).

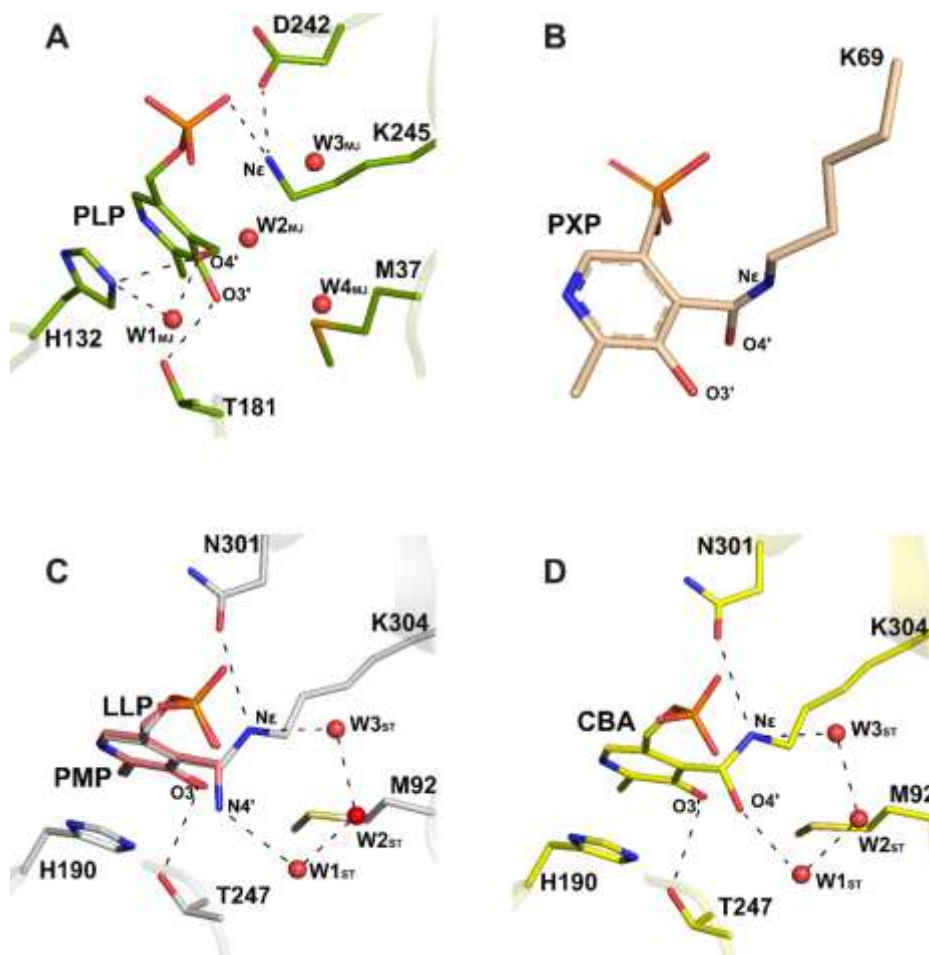


Figure 5: Geometry of interactions of the cofactor in the enzyme active sites. Active site residues and cofactor states are shown in stick representation A) Chain B of apoMjDC•PLP_{ALD} (PDB ID: 3F9T) is shown in green; B) PXP ligand showing the geometry of the CBA intermediate in the active site of ODC (PDB ID: 1SZR) is colored in beige; C) StDC active site showing partially occupied LLP (grey) and PMP (pink) (PDB ID: 4RIZ chain A); D) Reconstructed model of the CBA intermediate in StDC active site (yellow). In all the figures, nitrogen atoms are shown in blue and oxygen atoms are shown in red color; hydrogen bond interactions (< 3.2 Å), are displayed as dashed black lines. Waters are shown as red spheres. W1_{MJ}, W2_{MJ}, W3_{MJ} and W4_{MJ} are W482, W481, W721 and W646 in apoMjDC•PLP_{ALD}, respectively (PDB ID: 3F9T chain B); W1_{ST}, W2_{ST} and W3_{ST} are W841, W842 and W678 in StDC, respectively (PDB ID: 4RIZ chain A).

Structure based sequence alignment reflects the high degree of sequence and structural conservation of the catalytic and PLP binding residues between apoMjDC•PLP_{ALD} and StDC (Fig. S4) (rmsd ~2.9 Å over 384 equivalent C α atoms). Furthermore, the positioning of the pyridine rings

is largely identical between the two homologs (Fig. S8) and the non-bonded interactions reveal a binding mode consistent with that expected for an enzyme bound CBA complex (Oliveira et al., 2011). Thus, we envisaged a proposal for the structural basis of the mechanism of formation of the CBA in Group II decarboxylases from an analysis of the pyridoxal-P interactions in apoMjDC•PLP_{ALD} and the optimized CBA model in StDC. In this scheme, the transfer of a proton from N ζ to O4' for the formation of the CBA can be achieved by multiple pathways *viz*, direct transfer, or mediated *via* a neighboring residue or a water molecule (Fig. 5D and Scheme 2A, B). In the StDC-CBA model, the geometry of the donor N ζ and acceptor O4' atoms precludes a direct proton transfer between them since these heavy atoms are already juxtaposed in a sterically hindered conformation (Fig. 5D). Several theoretical studies also rule out the possibility of a direct proton transfer owing to the high activation barrier associated with such a mechanism (Oliveira et al., 2011; Salvà et al., 2003).

Next, we considered proton transfer by neighboring residues. The residues in the immediate environment of N ζ and O4' atoms are Thr247 (Thr181 in MjDC) and Met92 (Met37 in MjDC) (Fig. S8). The distances between N ζ and O4' from Thr247 O γ 1 are 5.0 Å and 3.9 Å, respectively. Furthermore, Thr247 is present on a rigid turn that restricts its movement ruling out the possibility of a threonine-mediated transfer. The S δ atom of Met92 side chain is positioned between the N ζ and O4', at a distance of 4 Å from the O4' and 4.7 Å from the N ζ . However, methionine is not known to be involved in proton transfer mechanisms. Furthermore, Met92 is not conserved and is substituted by Phe, Leu or Tyr residues in homologs (Fig. S4). Interestingly, substitution of Met37 with Phe in MjDC increased specific activity by 2-fold (Fig. 6). It appears that the hydrophobicity of the residue at this position is important for the activity or SB formation in Group II decarboxylases. The possibility of a Tyr residue mediating the proton transfer reaction in specific orthologs cannot be ruled out.

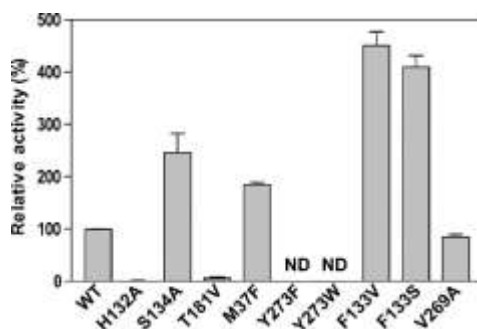


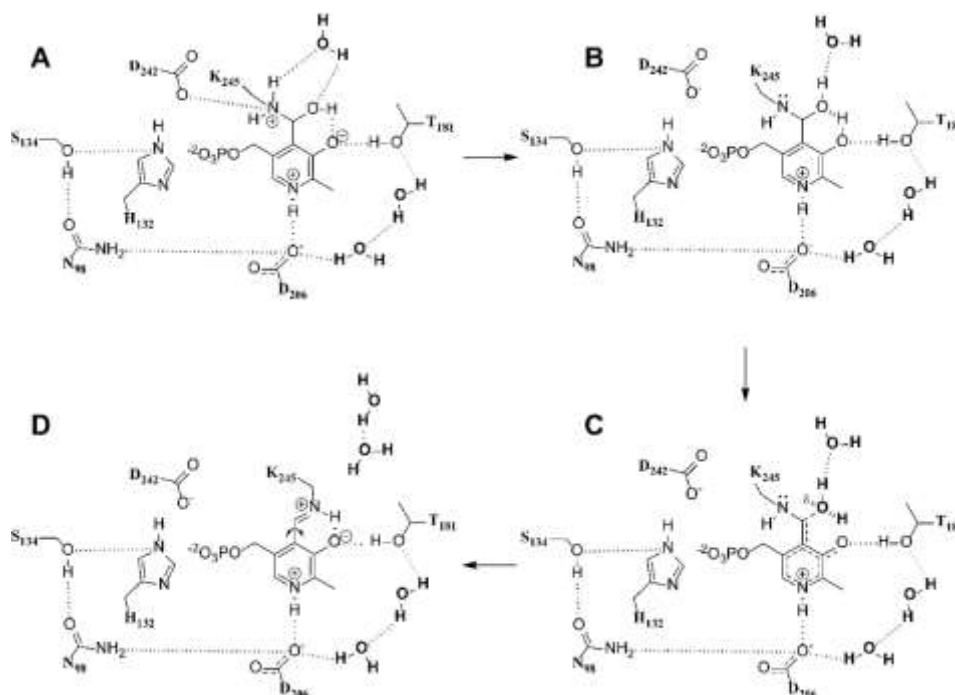
Figure 6: Relative activity of MjDC WT and mutants. The specific activity of the WT enzyme towards L-tyrosine is set to 100 %. The error bar represents the standard deviation between replicates. For the Tyr273 mutants (Y273F and Y273W) no detectable activity was observed at standard assay conditions, denoted as ND.

The alternate scenario is a water-mediated proton transfer. In apoMjDC•PLP_{ALD}, four water molecules are found within 5 Å radius of the N ζ and O4' atoms, suggesting a direct participation of water in proton transfer (Fig 5A). Remarkably, inspection of active sites across the 18 independent subunits in the StDC structures reveals the presence of an equivalent conserved water network comprising of three water molecules (W1_{ST}, W2_{ST} and W3_{ST}) appropriately positioned within a distance of 4 Å from the N ζ and O4' atoms (Fig. 5C). W1_{ST} is positioned at a distance of 2.7 Å from O4' while W2_{ST} is at 2.4 Å and 2.8 Å from W1_{ST} and W3_{ST}, respectively. W3_{ST} is 3.8 Å from N ζ , appropriate for transfer. An even closer distance between W3_{ST} and N ζ can be achieved by slight rotation around the C δ -C ϵ bond. Superposition of the active sites of MjDC on StDC shows that W1_{MJ} is ~2.0 Å from W1_{ST}, W2_{MJ} and W4_{MJ} are within ~2.5 Å from W2_{ST}, and W3_{MJ} is present at the exact position of W3_{ST} indicating a structural conserved water network (Fig. S8). Taken together, in the water-mediated proton transfer mechanism, one of the ammonium hydrogens of the N ζ is transferred to W3_{ST} (W3_{MJ}) with a hybridization change of N ζ from sp^3 to sp^2 (Scheme S1). Simultaneously, the proton gets transferred *via* the other water molecules (W1_{ST} and W2_{ST}) to O4' with concurrent migration of the shared proton (between O3' and O4') to the phenoxide ion (O3'), resulting in the formation of the CBA (Scheme 2B). Overall, the observed geometry of interactions between the enzyme, conserved waters and CBA is consistent with the general mechanism of a water-mediated proton transfer during SB formation (Oliveira et al., 2011; Salvà et al., 2003).

3.3.4 Dehydration and internal aldimine formation. The final step of the reaction is the formation of the internal aldimine by dehydration of the CBA intermediate. This requires the transfer of a proton from O3' to O4' leading to the formation of a zwitterionic quinonoid-like intermediate resulting in the loss of bond between C4'-O4' with subsequent release of a water molecule (Scheme 2C). The formation of the SB requires a rotational rearrangement of Lys245 such that the protonated N ζ atom is oriented nearly coplanar with PLP, making a hydrogen bond between the N ζ and the O3' atoms. The end result is a stable zwitterionic species with restoration of the aromaticity of the pyridinium ring and concomitant formation of the internal aldimine species (Scheme 2D) (Salvà et al., 2002; Salvà et al., 2003). The product of the reaction would resemble the structure of the cofactor in holoMjDC•LLP (Fig. 2C).

Examination of the cofactor binding pockets of the CBA-StDC model and holoMjDC•LLP suggests a probable route for internal aldimine formation from the carbinolamine intermediate. In the CBA model, the presence of the hydrogen bonds between W1_{ST} and the O4', and between Thr247 and the O3' would enable the migration of the proton from the O3' to O4' (Fig. 5D). Following this,

the partial negative charge on O3' is expected to be delocalized through the π system into the pyridine ring resulting in the formation of a quinonoid-like intermediate that facilitates the release of water (Scheme 2C) (Salvà et al., 2002; Salvà et al., 2003). Lastly, the C4-C4' bond undergoes a rotational rearrangement enabling the transfer of the hydrogen at the N ζ to the phenoxide O3', resulting in the formation of the SB (Scheme 2D).



Scheme 2: Proposed mechanism of internal aldimine formation in MjDC.

The pyridine ring also undergoes a relative reorientation involving a tilt of $\sim 6^\circ$ between the two forms (Fig. 7A). As a result, interactions between the O3' and C4' atoms of pyridoxal-P and the O γ of Thr181 and the C ϵ of Met37, respectively, is lost in the internal aldimine form where both residues adopt multiple conformations (Fig. 7A).

As expected of this scheme in the geometry of the internal aldimine state of holoMjDC•LLP, the N ζ and O3' atoms are at a distance of 2.5 Å, indicating the formation of the intra-molecular hydrogen bond (Fig. 2C, Scheme 2 D). Several other structures of Group II decarboxylases in the internal aldimine form are available in the PDB (PDB ID: 1JS6, 2OKK, 4OBU, 4RIT, 3K4O, 5HSJ). These share a similar cisoid conformation of the internal aldimine with that in MjDC suggesting that this conformation is the most abundant active conformation (Burkhard et al., 2001; Fenalti et al., 2007; Han et al., 2010; Williams et al., 2014; Zhu et al., 2016). In holoMjDC•LLP, this conformation is achieved by a rotation of the N ζ of Lys245 by $\sim 100^\circ$ around its χ_4 torsion angle with respect to the corresponding position in apoMjDC•PLP_{ALD}, resulting in the loss of the Lys245-Asp242 ion-pair interaction (Fig. 2C and D, Fig. 5A). The side chain of Asp242 now assumes dual conformations to

form interactions with N ϵ 2 of His244 and main chain amide of Gly94 (Fig. 1B and 7A). Asp242 is conserved within euryarchaeotic homologs, whereas, it is usually an Asn in other Group II decarboxylases (Fig. S9). Since these organisms dwell in harsh conditions that may destabilize polar interactions, an ion-pair interaction between Asp242 and Lys245 might provide a more stable interaction over a hydrogen bond in their native environment (Brininger et al., 2018; Stetter, 1999; Vieille and Zeikus, 2001). The propensity of Asp242 to switch conformations upon SB formation suggests a possible role for this residue in regulating the rate of SB formation in MjDC.

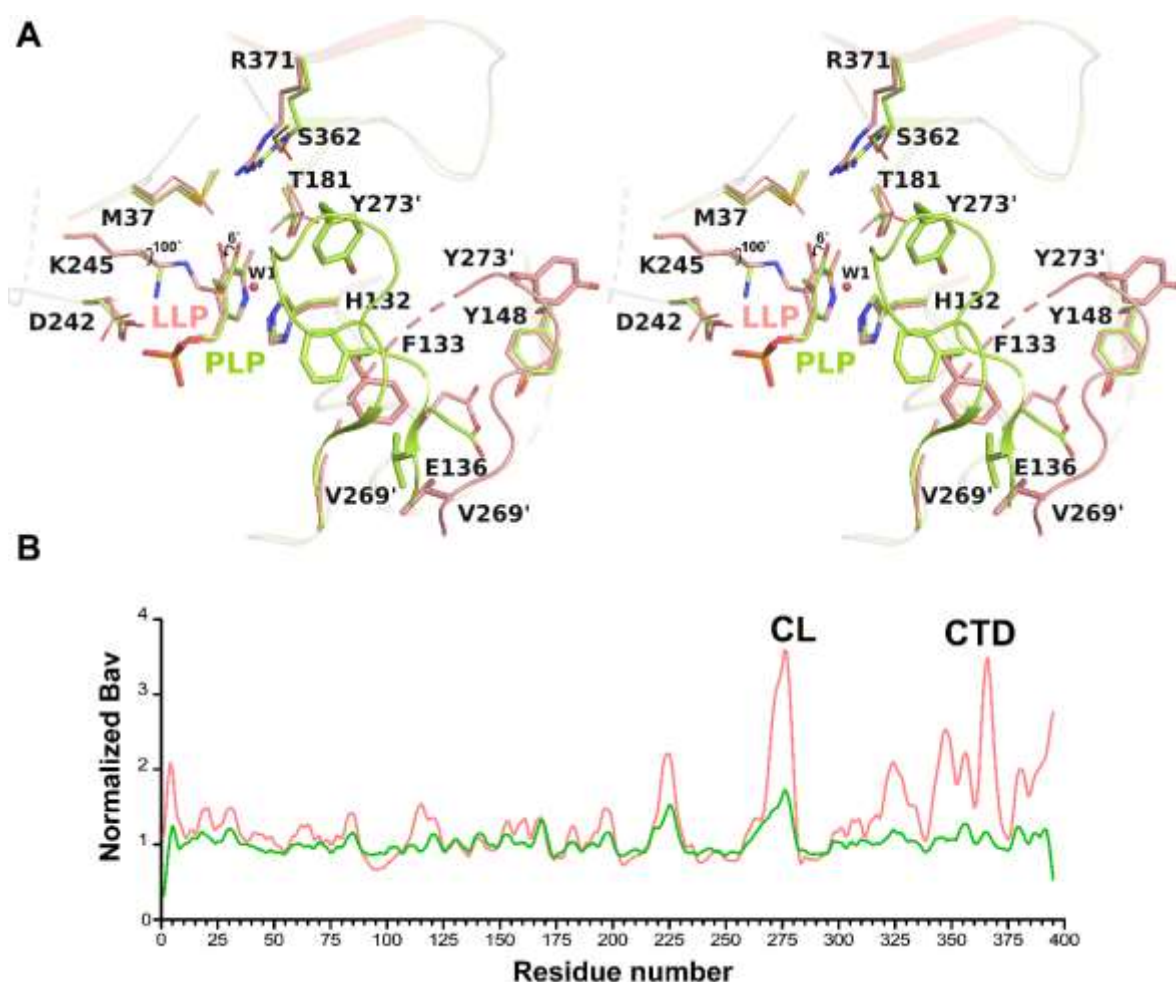


Figure 7: Open and closed states of MjDC showing the order-disorder transition. (A) Stereo diagram of the active site of apoMjDC•PLP_{ALD} (green) and holoMjDC•LLP (pink). Active site residues, PLP and LLP are represented in stick format. Water molecule is represented as a small red sphere. Rotational rearrangement (~100°) around the active site Lys245 and the tilt (6°) of the pyridine ring are shown. (F) Plot shows the B-factors of the C α atoms vs residue number in apoMjDC•PLP_{ALD} (green) and holoMjDC•LLP (pink). The CL and the CTD of the open state of holoMjDC•LLP display increased mobility relative to the closed state in apoMjDC•PLP_{ALD}.

3.4 Influence of an extended hydrogen-bonding network in regulating internal aldimine formation. Enzyme free pyridoxal-P is usually present with a deprotonated pyridine nitrogen (N1) and a protonated O3' at physiological pH in solution (Casasnovas et al., 2009; Chan-Huot et al., 2010). However, several experimental studies on fold-type I AATs have shown that the pyridine N1 exists in the protonated form in the internal aldimine state. The electrophilicity of the protonated N1-PLP enables formation of resonance stabilized quinonoid intermediates subsequent to external aldimine formation and affects catalytic function (Caulkins et al., 2014; Dajnowicz et al., 2017a; Dajnowicz et al., 2017b; Limbach et al., 2011; Toney, 2011). Furthermore, theoretical studies have shown that formation of a quinonoid-like intermediate is also a key feature that facilitates proton transfer between O3' and O4' and the nucleophilic attack step of internal aldimine formation (Salvà et al., 2002; Salvà et al., 2003). For instance, in porcine AAT it was demonstrated that the hydrogen bond network spanning from pyridine N1 to the bulk solvent through a conserved Asp222 (Asp206 in MjDC) directly influences the protonation state of N1 and that this protonation happens during internal aldimine formation (Dajnowicz et al., 2017a; Dajnowicz et al., 2017b). An identical network in human HDC was proposed to stabilize the charge on the conserved Asp (Asp206 in MjDC) upon quinonoid formation after the external aldimine formation. (Fernandes, 2017). Therefore, we were prompted to examine whether the protonation of N1-PLP *via* this network can similarly influence the internal aldimine formation step in MjDC.

In AAT, the protonation was inferred from direct visualization of a deuterium in a hydrogen bond between N1-PLP and the side chain of Asp222. Furthermore, observation of non-planarity of the SB bond relative to the pyridinium ring ($N\zeta-C4'-C4-C3$ torsion angle of 46°) in the internal aldimine state suggested that this torsion angle is affected by the electron-withdrawing ability of the pyridinium ring (Dajnowicz et al., 2017b). In holoMjDC•LLP, the SB $C4'=N\zeta$ bond is above the plane of the pyridinium ring with the $N\zeta-C4'-C4-C3$ torsion angle of 32° , consistent with the presence of a protonated N1-PLP (Fig. 2C). Here, the hydrogen bond between N1-PLP and the conserved Asp206 increases the pK_a of the N1 atom and stabilizes the pyridinium ring. Furthermore, Asp206 is coupled to a hydrogen-bonding network consisting of the side chains of Asn98, Ser134 and His132 that connects to the bulk solvent, reminiscent of the network in AAT (Fig. 8). It is conceivable that this hydrogen-bonding network coupled to the protonation state of N1-PLP in MjDC influences the electrophilicity of the cofactor. Interestingly, in apoMjDC•PLP_{ALD}, the aldehyde group (O4') of pyridoxal-P also interacts with this network *via* $W1_{MJ}$ and the side chain of His132 (Fig. 8). Between the apo- and holo-forms, the geometry of the extended hydrogen-bonding network remains invariant but for the presence of $W1_{MJ}$ in the apo-form (Fig. 8). Thus, these two

structures allow us to clearly identify the local environment connecting the protonation states of the network residues, the N1 atom, and the intra-molecular proton transfer pathway between the O4' and O3' in the extended delocalized π system of the cofactor. Any perturbation of this microenvironment is expected to significantly affect the rate of SB formation in MjDC, in particular, the nucleophilic attack step since the nucleophilicity of the C4' is dictated by the position of the intra-molecular shared proton (Scheme S2) (Casasnovas et al., 2009). Similar interactions of the O4' with a water molecule and the equivalent His residue in homologous apoALAS (5-aminolevulinate synthase, PDB ID: 5TXR), suggesting that the state that we observe here is a likely conserved functional state that precedes SB formation (Brown et al., 2018).

The residues constituting this network are conserved across the Group II decarboxylases (Fig. S4). For instance, in the orthologous human DDC (sequence identity of 16% with MjDC), this network is comprised of the side chains of the equivalent conserved residues His192, Ser194, Thr152, and Asp271, and a water molecule (Fig. S10). In the structures of the DDC apo-form (PDB ID: 3RBF, chain B) and the pyridoxal-P form (PDB ID: 3RBF chain A), the network is incomplete due to the absence of the connecting water molecule, whereas in the LLP forms (PDB ID: 3RCH chain A, 1JS6) and the external aldimine form (PDB ID: 1JS3) that contain this water, the hydrogen-bonding network is fully established (Fig. S10). We disrupted this network in MjDC by substituting the conserved His132 and Ser134 with Ala. The H132A mutant is devoid of activity and the spectra of the mutant clearly shows reduced PLP binding with significant changes in the keto-enol equilibrium. This is expected since H132 maintains strong stacking interactions with PLP. In contrast, the S134A mutant showed increase in specific activity by 2-fold, although there were no apparent changes in the spectroscopic property (Fig. 6 and S12). Perhaps waters from bulk solvent that can substitute for loss of the Ser OH can provide an alternate, more efficient path, for proton hopping. In essence, this network (referred to as network I) is expected to directly influence the protonation state of the pyridine N1 in other Group II decarboxylases as well.

A close examination of the cofactor binding pocket of MjDC revealed the presence of another as yet unreported hydrogen-bonding network that bridges the O3' atom of PLP with the N1-PLP *via* the side chain of the conserved Thr181 and two structurally conserved water molecules, W5_{MJ} and W6_{MJ} (Fig. 8). This network (referred to as network II) is seemingly conserved since it is also present in the crystal structures of other Group II decarboxylases (PDB ID: 2OKJ, 1JS3, 4E1O, 4RIT) (Fig S11) (Burkhard et al., 2001; Fenalti et al., 2007; Komori et al., 2012). Thr181 is completely conserved across the Group II decarboxylase family (Fig. S4). In several crystal structures, including that of holoMjDC•LLP, Thr181 can be found in varied conformations which probably correspond

to different protonation states of the cofactor. A dual role for the Thr residue in the stabilization of two different L-DOPA external aldimine tautomers was proposed in a QM/MM study of pig DDC where Thr acts as the hydrogen bond donor and acceptor for the oxoamine phenolate oxygen (PLP-O3[']) and the hydroxyimine phenolic hydroxyl group (PLP-O3[']-H), respectively (Lin et al., 2011). In order to examine the role of Thr at this position in MjDC, it was substituted by Val. The mutant shows 10-fold decrease in specific activity. However, the spectroscopic properties indicate a bound internal aldimine suggesting that a disruption of this network significantly influences catalysis (Fig. 6 and S12). Thus, it appears that in MjDC, network II involving the hydroxyl group of Thr181, the O3['] and the N1-PLP also influences the electronic state of PLP. In a comprehensive analysis of NMR structures of PLP and PLP model Schiff bases in solid state, Limbach et al., suggested that the protonation status of the phenol (O3[']) and the N1 groups of PLP are coupled with assistance from local proton donors (Limbach et al., 2011). Perhaps, a similar coupling of protonation states of the PLP O3['] and N1 atoms is mediated by Thr181. These findings suggest a novel role for Thr181 in influencing catalysis within Group II decarboxylases *via* network II.

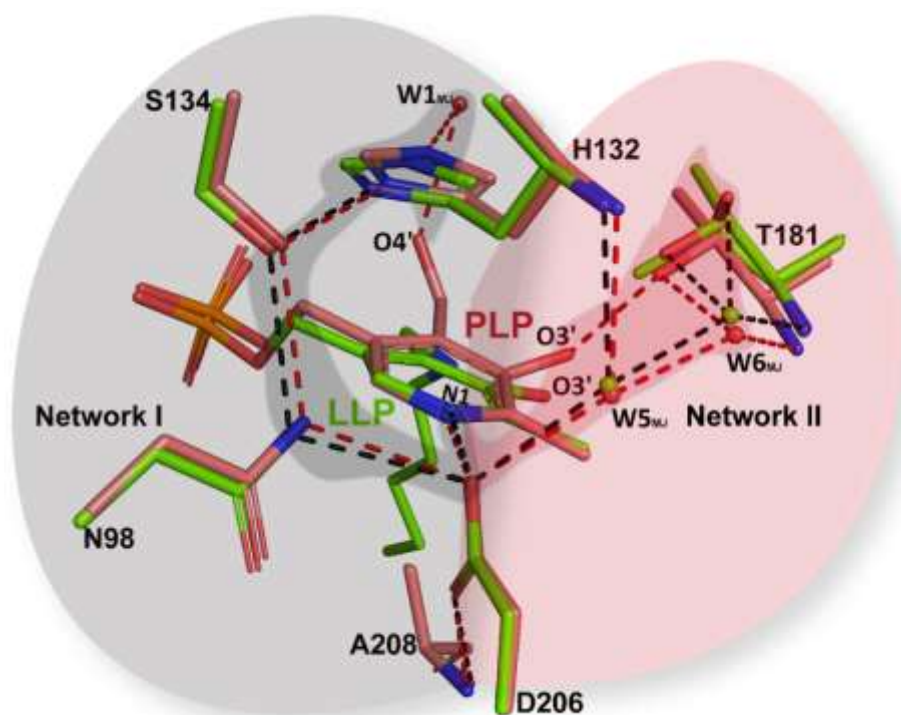


Figure 8: Extended hydrogen-bonding network of MjDC. Structural superposition of the active site residues of apoMjDC•PLP_{ALD} (pink) and holoMjDC•LLP (green). The complete extended hydrogen-bonding network (I and II) that connects the solvent to the N1-PLP and, the N1 to the O3['] is shown on grey and pink backgrounds, respectively. The interactions of the atoms involved in the inter-molecular proton transfer pathway are highlighted. Side chains involved in the extended hydrogen-bonding network are represented

in stick format. Water molecules from apoMjDC•PLP_{ALD} and holoMjDC•LLP are represented as red and green spheres, respectively. Hydrogen bond interactions (< 3.2 Å), are displayed as red dashed lines for apoMjDC•PLP_{ALD}, and black dashed lines for holoMjDC•LLP. W5_{MJ} and W6_{MJ} are W561, W524 in apoMjDC•PLP_{ALD}, respectively (PDB ID: 3F9T chain B).

Network I and II are connected to each other through the O δ 2 atom of the conserved Asp206 residue. The side chain orientation of Asp206 is completely preserved in this family due to the hydrogen bond (3.0 Å) between the O δ 1 atom and the main chain amide of a conserved Ala208 (Fig. 8). Together, the complete extended hydrogen-bonding network (I and II) that connects the solvent to the N1-PLP and, the N1-PLP to the O3', provides a microenvironment that influences the protonation state of PLP for the desired electronic configuration during internal aldimine formation or the subsequent decarboxylation reaction. Certainly in PLP based catalysis, cofactor and substrate binding trigger multiple inter- and intra-molecular proton transfers facilitated by selective protonation of key active site residues that fine tune catalysis by modulating one electronic configuration of the cofactor over another (Casasnovas et al., 2009; Casasnovas et al., 2012; Dajnowicz et al., 2017b; Griswold and Toney, 2011; Limbach et al., 2011; Toney, 2005).

3.5 Rearrangements in the PLP binding pocket regulates catalytic loop dynamics. Binding of pyridoxal-P to the apo-form of Group II decarboxylases is expected to act as an additional regulatory mechanism for its function and is usually accompanied by conformational changes in the protein (Giardina et al., 2011; Kass et al., 2014; Nishio et al., 2010). Spectrophotometric evidence from homologous *E.coli* GAD and SHMT suggest that binding of pyridoxal-P is initially driven by its phosphate arm to give an intermediate structure (apoE•PLP_{ALD}). Internal aldimine formation is accompanied by further conformational changes in the protein (Chen et al., 1998; Malerba et al., 2007). The nature and type or scale of these conformational changes upon internal aldimine formation are largely unidentified because of the lack of relevant structural snapshots of the apo- and holo-forms.

In Group II decarboxylases, the CL is an inherently flexible segment that hosts a catalytic Tyr residue and is generally disordered both in the apo- and holo-forms, rendering the active site “open” (Bertoldi et al., 2002; Burkhard et al., 2001; Fenalti et al., 2007; Giardina et al., 2011; Kass et al., 2014; Komori et al., 2012; Zhu et al., 2016). Nevertheless, in the external aldimine forms, the CL is known to form a closed active site pocket (Fenalti et al., 2007; Komori et al., Fernandes et al., 2017). The primary role of the conformational changes associated with a disorder-to-order transition of the CL is to bring the conserved catalytic proton donor residue Tyr (Tyr273' in MjDC) in close

proximity to the C α of the transition state intermediate to yield the product amine. Additionally, the dynamics of the CL may regulate substrate ingress and product egress (Fenalti et al., 2007; Komori et al., Fernandes et al., 2017). The lengths and composition of the CL region (13-24 residues, Fig. 3B) are divergent across the family and is likely to differentially affect its dynamics across orthologs. For instance, the greater flexibility of the CL of hGAD65 with respect to that in the hGAD67 isoform promoted a side reaction that resulted in the auto-inactivation of the former with the release of the cofactor (Fenalti et al., 2007; Langendorf et al., 2013). While most studies reported are with respect to changes during external aldimine formation, similar regulatory roles for the CL upon pyridoxal-P binding and internal aldimine formation cannot be ignored.

Interestingly, the CL of MjDC undergoes large conformational rearrangements (rmsd \sim 7.3 Å) between the apo- and holo-forms suggesting that CL dynamics may be influenced by conformational rearrangements in the PLP binding domain (Fig. 3A). In the only other reported structure of an apoE•PLP_{ALD} intermediate (human DDC), the CL is disordered (Giardina et al., 2011). Furthermore, in most of the available homologous holoE•LLP structures representing the hypothetical open state (PDB ID: 1JS6, 2OKK, 4OBU, 4RIT, 3K4O, 5HSJ), a major fraction of the CL regions is disordered (Burkhard et al., 2001; Fenalti et al., 2007; Han et al., 2010; Kass et al., 2014; Williams et al., 2014; Zhu et al., 2016). In contrast, the CL in apoMjDC•PLP_{ALD} is fully ordered and in the “closed” form (Fig. 3A). The CL in the closed form is primarily anchored by two hydrogen bonds, namely, between the OH of Tyr273' and the main chain amide of Phe133 and between the main chain carbonyl of Tyr273' and O γ 1 of Ser362 (Fig. 3E) (Table S1). Consequently, the active site cavity is completely shielded from the solvent (Fig. 3C and S2C). In the holoMjDC•LLP, we were able to clearly identify and build 9 out of 13 residues of the CL, including the catalytic Tyr273'. Using these positions, we then modelled the missing 4 residues to provide a reasonably unambiguous conformation of the usually disordered CL segment (Fig. S13). The OH atom of the catalytic Tyr273' undergoes the largest displacement of \sim 14 Å (Fig. 3A) away from the active site resulting in an “open” conformation (Fig. 3D and S2B). Accordingly, the presence of the ordered CL in both apo- and holo-forms of the same enzyme allowed us to describe structural determinants of the dynamics of the CL region in response to internal aldimine formation, for the first time.

Comparisons of the cofactor binding sites of both forms showed that the pyridine ring tilts by \sim 6°. Secondly, a significant concerted rearrangement of side chain orientations involving residues Phe133, Glu136 and Val269' occurs. Other minor rearrangements include side chains of Arg371, Ser362 and the previously described changes in Thr181 and Met37 (Fig. 7A). These conformational changes are presumably coupled to the tilt of the pyridine ring and internal aldimine formation. It

appears that the conformational change of the CL is primarily triggered by the large reorientation of the Phe133 side chain and propagated *via* steric interactions with residue Val269'. The side chain of the neighboring Glu136 also undergoes reorientation to form a new hydrogen bond with the OH of Tyr148 (Fig. 3F). As a result, the CL in holoMjDC•LLP assumes the open conformation exposing the active site to the solvent (Fig. 3D and S2B). The open conformation is primarily stabilized by stacking interactions between the catalytic Tyr273' and Tyr148 residue (Fig. 3F). Furthermore, in the open conformation, the CL is less ordered than that in the closed form since there is a relative loss of non-bonded interactions between the CL region and the rest of the protein (Table S1). This is manifested as the occurrence of multiple conformations of side chains in some residues, poorly defined side chain electron densities and an overall increase in B-factor value of the residues (Fig. 7). A comparison of B-factors between the two forms indicates that the CL and the CTD of the open form displays increased mobility relative to the rest of the protein (Fig. 7B). The increase in the entropy of the CTD in response to changes in CL conformation was observed earlier in human and *E.coli* GADs (Capitani et al., 2003; Fenalti et al., 2007; Gut et al., 2006; Kass et al., 2014; Langendorf et al., 2013). Based on these observations, we believe that MjDC might regulate substrate access to the active site after internal aldimine formation by promoting the transition from a closed to an open state.

Remarkably, substitution mutants of F133V and F133S showed a 4-fold increase in specific activity compared to the WT, whereas V269A had little effect on specific activity (Fig. 6). Therefore, we propose that the dynamics of the CL itself may be intimately linked to subtle structural changes in the cofactor binding pocket and is primarily mediated by the conformational rearrangement of Phe133 in MjDC. A similar role for the equivalent residue was proposed in the auto-inactivation of human GADs (Phe283) where substitutions and chimeric proteins with different CL segments showed that the composition of the loop as well as its packing environment influences CL dynamics (Fenalti et al., 2007). The substitution of Tyr273 to Phe or Trp in MjDC resulted in complete loss of decarboxylation activity (Fig. 6). Nevertheless, our data highlight the crucial role of Tyr273' in stabilizing the different conformations of the CL apart from its catalytic function. This argument is supported by kinetic data from the Y334F mutant of pig DDC wherein a reduction in the rate of decarboxylation is a result of poor substrate binding (increased K_m for larger substrates such as 5-hydroxytryptophan over L-DOPA) (Bertoldi et al., 2002). Similarly, altering the loop length of a *Lactobacillus* GAD affected overall activity without fully inactivating the enzyme (Huang et al., 2018). In summary, the CL acts like a gate to the active site in Group II decarboxylases and

inappropriate conformations of the CL induced by interactions of the catalytic Tyr may affect catalytic properties by physically impeding substrate entry/exit.

4. Conclusions. The results from the experimental snapshots observed here allows us to propose mechanistic roles of specific residues and water molecules in each step during the formation of the internal aldimine in Group II decarboxylases. Firstly, we demonstrate structural evidence for a water-mediated internal aldimine formation in an enzyme environment. Secondly, a conserved extended hydrogen-bonding network that includes second shell residues around PLP appears to influence internal aldimine formation and activation. Further, structural changes associated with internal aldimine formation, specifically, the rotational rearrangement of the active site Lys and the tilt of the pyridine ring is important for inducing the catalytically competent CL conformation of MjDC. This feature maybe general to homologous Group II decarboxylases. The data also indicate a plausible role for the catalytic Tyr in influencing CL dynamics. The unforeseen transition from the closed conformation of apoMjDC•PLP_{ALD} to the open form of holoMjDC•LLP sets the stage for further studies to include the role of CL dynamics during internal aldimine formation. We believe that these structural observations support a ‘conformational selection’ model during internal aldimine formation in Group II decarboxylases and that future QM/MM studies must employ these features in order to propose an atomistic model of this mechanism.

Author contributions

SCG carried out the experiments and analyzed the data. NM carried out data analysis, supervised the study and wrote the manuscript jointly with SCG.

Acknowledgments

Data were collected at BM14 beamline (ESRF, Grenoble). We thank Hassan Belrhali and Babu A. Manjasetty for help with data collection. Data collection at ESRF was funded by the BM14 project, a collaboration between Department of Biotechnology (DBT), Ministry of Science and Technology, Government of India, European Molecular Biology Laboratory (EMBL), and ESRF. We thank the DBT for funding. The Macromolecular X-ray Diffraction Facility and the DST-FIST Facility at IIT Madras, are acknowledged. CGS is supported by funding from the Council of Industrial and Scientific Research (CSIR) and the Ministry of Human Resource and Development (MHRD), Government of India.

Table 1. Crystallographic data collection and refinement statistics

Data set	holoMjDC•LLP
PDB ID	6JY1
Data collection	
Wavelength (Å)	0.976
Space group	P4 ₃ 2 ₁ 2
Unit cell parameters	
a, b, c (Å)	98.6, 98.6, 122.3
Molecules in asymmetric unit	1
Resolution range (Å) ^a	51.96 – 1.72 (1.78 – 1.72)
R _{merge} on I (%) ^a	7.0 (98.4)
Mean (I/σ (I)) ^a	18.6 (2.1)
Total reflections	531270
No. of unique reflections	64532
Completeness (%) ^a	100 (96.3)
Multiplicity ^a	8.2 (6.4)
CC _{1/2} ^{a,b}	99.8 (70.0)
Wilson B-factor (Å ²)	23.7
Model and refinement statistics	
Free R reflections (%)	5.0
R _{work} /R _{free} (%) ^c	16.3/18.9
Non-hydrogen protein atoms	3142
Solvent atoms	286
Ligand atoms	42
Mean B value, all atoms (Å ²)	32
RMS deviations from ideal geometry	
Bond angle (°)	1.26
Bond length (Å)	0.01
Ramachandran plot analysis	
Favored (%)	96.1
Allowed (%)	3.9
Disallowed (%)	0.0

^a Value in parentheses refer to the highest resolution shell.

^b CC_{1/2} is the correlation coefficient of the mean intensities between two random half-sets of data (Adams et al., 2011).

^c $R_{\text{work}} = \frac{\sum |F_{\text{obs}}| - |F_{\text{calc}}|}{\sum |F_{\text{obs}}|}$, R_{free} is calculated for a set of 5% of reflections randomly chosen and were not used for refinement; R_{work} is calculated for the remaining reflections.

References

- Adams, P.D., Afonine, P.V., Bunkoczi, G., Chen, V.B., Echols, N., Headd, J.J., Hung, L.W., Jain, S., Kapral, G.J., Grosse Kunstleve, R.W., McCoy, A.J., Moriarty, N.W., Oeffner, R.D., Read, R.J., Richardson, D.C., Richardson, J.S., Terwilliger, T.C., Zwart, P.H., 2011. The Phenix software for automated determination of macromolecular structures. *Methods* 55, 94-106.
- B:urgi, H.B., Dunitz, J.D., Lehn, J.M., Wipff, G., 1974. Stereochemistry of reaction paths at carbonyl centres. *Tetrahedron* 30, 1563-1572.

- Battye, T.G., Kontogiannis, L., Johnson, O., Powell, H.R., Leslie, A.G., 2011. iMOSFLM: a new graphical interface for diffraction-image processing with MOSFLM. *Acta Crystallogr. D Biol. Crystallogr.* 67, 271-281.
- Bertoldi, M., 2014. Mammalian Dopa decarboxylase: structure, catalytic activity and inhibition. *Arch. Biochem. Biophys.* 546, 1-7.
- Bertoldi, M., Gonsalvi, M., Contestabile, R., Voltattorni, C.B., 2002. Mutation of tyrosine 332 to phenylalanine converts dopa decarboxylase into a decarboxylation-dependent oxidative deaminase. *J. Biol. Chem.* 277, 36357-36362.
- Bourquin, F., Riezman, H., Capitani, G., Grutter, M.G., 2010. Structure and function of sphingosine-1-phosphate lyase, a key enzyme of sphingolipid metabolism. *Structure* 18, 1054-1065.
- Brininger, C., Spradlin, S., Cobani, L., Evilia, C., 2018. The more adaptive to change, the more likely you are to survive: Protein adaptation in extremophiles. *Semin. Cell. Dev. Biol.* 84, 158-169.
- Brown, B.L., Kardon, J.R., Sauer, R.T., Baker, T.A., 2018. Structure of the Mitochondrial Aminolevulinic Acid Synthase, a Key Heme Biosynthetic Enzyme. *Structure* 26, 580-589 e584.
- Burkhard, P., Dominici, P., Borri-Voltattorni, C., Jansonius, J.N., Malashkevich, V.N., 2001. Structural insight into Parkinson's disease treatment from drug-inhibited DOPA decarboxylase. *Nat. Struct. Mol. Biol.* 8, 963-967.
- Capitani, G., De Biase, D., Aurizi, C., Gut, H., Bossa, F., Grutter, M.G., 2003. Crystal structure and functional analysis of *Escherichia coli* glutamate decarboxylase. *EMBO J.* 22, 4027-4037.
- Casasnovas, R., Salvà, A., Frau, J., Donoso, J., Muñoz, F., 2009. Theoretical study on the distribution of atomic charges in the Schiff bases of 3-hydroxypyridine-4-aldehyde and alanine. The effect of the protonation state of the pyridine and imine nitrogen atoms. *Chem. Phys.* 355, 149-156.
- Casasnovas, R., Adrover, M., Ortega-Castro, J., Frau, J., Donoso, J., Muñoz, F., 2012. C-H Activation in Pyridoxal-5'-phosphate Schiff Bases: The Role of the Imine Nitrogen. A Combined Experimental and Computational Study. *J. Phys. Chem. B* 116, 10665-10675.
- Caulkins, B.G., Bastin, B., Yang, C., Neubauer, T.J., Young, R.P., Hilario, E., Huang, Y.M., Chang, C.E., Fan, L., Dunn, M.F., Marsella, M.J., Mueller, L.J., 2014. Protonation states of the tryptophan synthase internal aldimine active site from solid-state NMR spectroscopy: direct observation of the protonated Schiff base linkage to pyridoxal-5'-phosphate. *J. Am. Chem. Soc.* 136, 12824-12827.
- Chan-Huot, M., Sharif, S., Tolstoy, P.M., Toney, M.D., Limbach, H.H., 2010. NMR studies of the stability, protonation States, and tautomerism of (13)C- AND (15)N-labeled aldimines of the coenzyme pyridoxal 5'-phosphate in water. *Biochemistry* 49, 10818-10830.
- Chen, C.H., Wu, S.J., Martin, D.L., 1998. Structural characteristics of brain glutamate decarboxylase in relation to its interaction and activation. *Arch. Biochem. Biophys.* 349, 175-182.
- Chen, V.B., Arendall, W.B., 3rd, Headd, J.J., Keedy, D.A., Immormino, R.M., Kapral, G.J., Murray, L.W., Richardson, J.S., Richardson, D.C., 2010. MolProbity: all-atom structure validation for macromolecular crystallography. *Acta Crystallogr. D Biol. Crystallogr.* 66, 12-21.
- Dajnowicz, S., Parks, J.M., Hu, X., Gesler, K., Kovalevsky, A.Y., Mueser, T.C., 2017a. Direct evidence that an extended hydrogen-bonding network influences activation of pyridoxal 5'-phosphate in aspartate aminotransferase. *J. Biol. Chem.* 292, 5970-5980.
- Dajnowicz, S., Johnston, R.C., Parks, J.M., Blakeley, M.P., Keen, D.A., Weiss, K.L., Gerlits, O., Kovalevsky, A., Mueser, T.C., 2017b. Direct visualization of critical hydrogen atoms in a pyridoxal 5'-phosphate enzyme. *Nat. Commun.* 8, 955.
- Denesyuk, A.I., Denessiouk, K.A., Korpela, T., Johnson, M.S., 2003. Phosphate group binding "cup" of PLP-dependent and non-PLP-dependent enzymes: leitmotif and variations. *Biochim. Biophys. Acta* 1647, 234-238.
- Ding, Y.-q., Cui, Y.-z., Li, T.-d., 2015. New Views on the Reaction of Primary Amine and Aldehyde from DFT Study. *J. Phys. Chem. A* 119, 4252-4260.
- Dutyshev, D.I., Darii, E.L., Fomenkova, N.P., Pechik, I.V., Polyakov, K.M., Nikonov, S.V., Andreeva, N.S., Sukhareva, B.S., 2005. Structure of *Escherichia coli* glutamate decarboxylase (GADalpha) in complex with glutarate at 2.05 angstroms resolution. *Acta Crystallogr. D Biol. Crystallogr.* 61, 230-235.
- Emsley, P., Cowtan, K., 2004. Coot: model-building tools for molecular graphics. *Acta Crystallogr. D Biol. Crystallogr.* 60, 2126-2132.

- Evans, P.R., 2011. An introduction to data reduction: space-group determination, scaling and intensity statistics. *Acta Crystallogr. D Biol. Crystallogr.* 67, 282-292.
- Fenalti, G., Law, R.H., Buckle, A.M., Langendorf, C., Tuck, K., Rosado, C.J., Faux, N.G., Mahmood, K., Hampe, C.S., Banga, J.P., Wilce, M., Schmidberger, J., Rossjohn, J., El-Kabbani, O., Pike, R.N., Smith, A.I., Mackay, I.R., Rowley, M.J., Whisstock, J.C., 2007. GABA production by glutamic acid decarboxylase is regulated by a dynamic catalytic loop. *Nat. Struct. Mol. Biol.* 14, 280-286.
- Fernandes, H.S., Ramos, M.J., Cerqueira, N.M., 2017. The Catalytic Mechanism of the Pyridoxal-5'-phosphate-Dependent Enzyme, Histidine Decarboxylase: A Computational Study. *Chem. A Eur. J.*
- Giardina, G., Montioli, R., Gianni, S., Cellini, B., Paiardini, A., Voltattorni, C.B., Cutruzzolà, F., 2011. Open conformation of human DOPA decarboxylase reveals the mechanism of PLP addition to Group II decarboxylases. *Proc. Natl. Acad. Sci.* 108, 20514-20519.
- Griswold, W.R., Toney, M.D., 2011. Role of the pyridine nitrogen in pyridoxal 5'-phosphate catalysis: activity of three classes of PLP enzymes reconstituted with deazapyridoxal 5'-phosphate. *J. Am. Chem. Soc.* 133, 14823-14830.
- Gut, H., Pennacchietti, E., John, R.A., Bossa, F., Capitani, G., De Biase, D., Grutter, M.G., 2006. *Escherichia coli* acid resistance: pH-sensing, activation by chloride and autoinhibition in GadB. *EMBO J.* 25, 2643-2651.
- Gut, H., Dominici, P., Pilati, S., Astegno, A., Petoukhov, M.V., Svergun, D.I., Grutter, M.G., Capitani, G., 2009. A common structural basis for pH- and calmodulin-mediated regulation in plant glutamate decarboxylase. *J. Mol. Biol.* 392, 334-351.
- Han, Q., Ding, H., Robinson, H., Christensen, B.M., Li, J., 2010. Crystal structure and substrate specificity of *Drosophila* 3,4-dihydroxyphenylalanine decarboxylase. *PloS one* 5, e8826.
- Holm, L., Laakso, L.M., 2016. Dali server update. *Nucleic Acids Res.* 44, W351-355.
- Huang, J., Fang, H., Gai, Z.C., Mei, J.Q., Li, J.N., Hu, S., Lv, C.J., Zhao, W.R., Mei, L.H., 2018. *Lactobacillus brevis* CGMCC 1306 glutamate decarboxylase: Crystal structure and functional analysis. *Biochem. Biophys. Res. Commun.* 503, 1703-1709.
- Ishii, S., Hayashi, H., Okamoto, A., Kagamiyama, H., 1998. Aromatic L-amino acid decarboxylase: conformational change in the flexible region around Arg334 is required during the transaldimination process. *Protein science : a publication of the Protein Society* 7, 1802-1810.
- Jackson, L.K., Baldwin, J., Akella, R., Goldsmith, E.J., Phillips, M.A., 2004. Multiple active site conformations revealed by distant site mutation in ornithine decarboxylase. *Biochemistry* 43, 12990-12999.
- Kack, H., Sandmark, J., Gibson, K., Schneider, G., Lindqvist, Y., 1999. Crystal structure of diaminopelargonic acid synthase: evolutionary relationships between pyridoxal-5'-phosphate-dependent enzymes. *J. Mol. Biol.* 291, 857-876.
- Kass, I., Hoke, D.E., Costa, M.G., Reboul, C.F., Porebski, B.T., Cowieson, N.P., Leh, H., Pennacchietti, E., McCoe, J., Kleifeld, O., Borri Voltattorni, C., Langley, D., Roome, B., Mackay, I.R., Christ, D., Perahia, D., Buckle, M., Paiardini, A., De Biase, D., Buckle, A.M., 2014. Cofactor-dependent conformational heterogeneity of GAD65 and its role in autoimmunity and neurotransmitter homeostasis. *Proc. Natl. Acad. Sci.* 111, E2524-2529.
- Kezmarsky, N.D., Xu, H., Graham, D.E., White, R.H., 2005. Identification and characterization of a L-tyrosine decarboxylase in *Methanocaldococcus jannaschii*. *Biochim. Biophys. Acta* 1722, 175-182.
- Komori, H., Nitta, Y., Ueno, H., Higuchi, Y., 2012. Structural study reveals that Ser-354 determines substrate specificity on human histidine decarboxylase. *J. Biol. Chem.* 287, 29175-29183.
- Kumar, R., 2016. Evolutionary Trails of Plant Group II Pyridoxal Phosphate-Dependent Decarboxylase Genes. *Front. Plant. Sci.* 7, 1268.
- Langendorf, C.G., Tuck, K.L., Key, T.L., Fenalti, G., Pike, R.N., Rosado, C.J., Wong, A.S., Buckle, A.M., Law, R.H., Whisstock, J.C., 2013. Structural characterization of the mechanism through which human glutamic acid decarboxylase auto-activates. *Biosci. Rep* 33, 137-144.
- Lebedev, A.A., Vagin, A.A., Murshudov, G.N., 2008. Model preparation in MOLREP and examples of model improvement using X-ray data. *Acta Crystallogr. D Biol. Crystallogr.* 64, 33-39.
- Limbach, H.H., Chan-Huot, M., Sharif, S., Tolstoy, P.M., Shenderovich, I.G., Denisov, G.S., Toney, M.D., 2011. Critical hydrogen bonds and protonation states of pyridoxal 5'-phosphate revealed by NMR. *Biochim. Biophys. Acta* 1814, 1426-1437.

- Lin, Y.L., Gao, J., Rubinstein, A., Major, D.T., 2011. Molecular dynamics simulations of the intramolecular proton transfer and carbanion stabilization in the pyridoxal 5'-phosphate dependent enzymes L-dopa decarboxylase and alanine racemase. *Biochim. Biophys. Acta* 1814, 1438-1446.
- Malerba, F., Bellelli, A., Giorgi, A., Bossa, F., Contestabile, R., 2007. The mechanism of addition of pyridoxal 5'-phosphate to *Escherichia coli* apo-serine hydroxymethyltransferase. *The Biochem J.* 404, 477-485.
- McLean, C.J., Marles-Wright, J., Custodio, R., Lowther, J., Kennedy, A.J., Pollock, J., Clarke, D.J., Brown, A.R., Campopiano, D.J., 2017. Characterization of homologous sphingosine-1-phosphate lyase isoforms in the bacterial pathogen *Burkholderia pseudomallei*. *J. Lipid Res.* 58, 137-150.
- Metzler, D.E., Christen, P., 1985. *Transaminases* Wiley, New York.
- Murshudov, G.N., Vagin, A.A., Dodson, E.J., 1997. Refinement of macromolecular structures by the maximum-likelihood method. *Acta Crystallogr. D Biol. Crystallogr.* 53, 240-255.
- Nishio, K., Ogasahara, K., Morimoto, Y., Tsukihara, T., Lee, S.J., Yutani, K., 2010. Large conformational changes in the *Escherichia coli* tryptophan synthase beta(2) subunit upon pyridoxal 5'-phosphate binding. *FEBS J.* 277, 2157-2170.
- Oliveira, E.F., Cerqueira, N.M., Fernandes, P.A., Ramos, M.J., 2011. Mechanism of formation of the internal aldimine in pyridoxal 5'-phosphate-dependent enzymes. *J. Am. Chem. Soc.* 133, 15496-15505.
- Paiardini, A., Contestabile, R., Buckle, A.M., Cellini, B., 2014. PLP-dependent enzymes. *Biomed Res. Int.* 2014, 856076.
- Pennacchietti, E., Lammens, T.M., Capitani, G., Franssen, M.C., John, R.A., Bossa, F., De Biase, D., 2009. Mutation of His465 alters the pH-dependent spectroscopic properties of *Escherichia coli* glutamate decarboxylase and broadens the range of its activity toward more alkaline pH. *J. Biol. Chem.* 284, 31587-31596.
- Percudani, R., Peracchi, A., 2003. A genomic overview of pyridoxal-phosphate-dependent enzymes. *EMBO Rep.* 4, 850-854.
- Pettersen, E.F., Goddard, T.D., Huang, C.C., Couch, G.S., Greenblatt, D.M., Meng, E.C., Ferrin, T.E., 2004. UCSF Chimera--a visualization system for exploratory research and analysis. *J. Comput. Chem.* 25, 1605-1612.
- Phan, A.P., Ngo, T.T., Lenhoff, H.M., 1983. Tyrosine decarboxylase. Spectrophotometric assay and application in determining pyridoxal-5'-phosphate. *Appl. Biochem. Biotechnol.* 8, 127-133.
- Raasakka, A., Mahootchi, E., Winge, I., Luan, W., Kursula, P., Haavik, J., 2018. Structure of the mouse acidic amino acid decarboxylase GADL1. *Acta Crystallogr. F Struct. Biol. Commun.* 74, 65-73.
- Richard, J.P., Amyes, T.L., Crujeiras, J., Rios, A., 2009. Pyridoxal 5'-phosphate: electrophilic catalyst extraordinaire. *Curr. Opin. Chem. Biol.* 13, 475-483.
- Robert, X., Gouet, P., 2014. Deciphering key features in protein structures with the new ENDscript server. *Nucleic Acids Res.* 42, W320-324.
- Salvà, A., Donoso, J., Frau, J., Muñoz, F., 2002. Theoretical studies on Schiff base formation of vitamin b6 analogues. *J. Mol. Struct.: THEOCHEM* 577, 229-238.
- Salvà, A., Donoso, J., Frau, J., Muñoz, F., 2003. DFT Studies on Schiff Base Formation of Vitamin B6 Analogues. *J. Phys. Chem. A* 107, 9409-9414.
- Sandmeier, E., Hale, T.I., Christen, P., 1994. Multiple evolutionary origin of pyridoxal-5'-phosphate-dependent amino acid decarboxylases. *Eur. J. Biochem.* 221, 997-1002.
- Schirch, L., Slotter, R.A., 1966. Spectral Properties of Schiff Bases of Amino Acid Esters with Pyridoxal and Pyridoxal N-Methochloride in Ethanol*. *Biochemistry* 5, 3175-3181.
- Schneider, G., Kack, H., Lindqvist, Y., 2000. The manifold of vitamin B6 dependent enzymes. *Structure* 8, R1-6.
- Seiler, C.Y., Park, J.G., Sharma, A., Hunter, P., Surapaneni, P., Sedillo, C., Field, J., Algar, R., Price, A., Steel, J., Throop, A., Fiocco, M., LaBaer, J., 2014. DNASU plasmid and PSI:Biography-Materials repositories: resources to accelerate biological research. *Nucleic Acids Res.* 42, D1253-1260.
- Sevilla, J.M., Blazquez, M., Dominguez, M., García-Blanco, F., 1992. A study of the Schiff base formed between pyridoxal-5'-phosphate and poly-L-lysine of low polymerization degree. *J. Chem. Soc., Perkin Trans. 2*, 921-926.

- Snell, E.E., 1971. Analogs of Pyridoxal or Pyridoxal Phosphate: Relation of Structure to Binding with Apoenzymes and to Catalytic Activity., p. 265-290, in: R. S. Harris, et al., Eds.), *Vitamins & Hormones*, Academic Press.
- Sonnet, P.E., Mascavage, L.M., Dalton, D.R., 2008. The first steps. The attack on the carbonyl carbon of pyridoxal cofactor in pyridoxal-dependent enzymes. *Bioorg. Med. Chem. Lett.* 18, 744-748.
- Stetter, K.O., 1999. Extremophiles and their adaptation to hot environments. *FEBS Lett.* 452, 22-25.
- Toney, M.D., 2005. Reaction specificity in pyridoxal phosphate enzymes. *Arch. Biochem. Biophys.* 433, 279-287.
- Toney, M.D., 2011. Controlling reaction specificity in pyridoxal phosphate enzymes. *Biochim. Biophys. Acta* 1814, 1407-1418.
- Vieille, C., Zeikus, G.J., 2001. Hyperthermophilic Enzymes: Sources, Uses, and Molecular Mechanisms for Thermostability. *Microbiol. Mol. Biol. Rev.* 65, 1.
- von Stosch, A.G., 1996. Aspartate aminotransferase complexed with erythro-beta-hydroxyaspartate: crystallographic and spectroscopic identification of the carbinolamine intermediate. *Biochemistry* 35, 15260-15268.
- Wada, H., Taketoshi, M., Imamura, I., Tanaka, T., Horio, Y., Taguchi, Y., Fukui, H., 1990. Mammalian histidine decarboxylase and dopa decarboxylase. *Ann. N. Y. Acad. Sci.* 585, 145-161.
- Wang, Y., Xu, H., White, R.H., 2014. β -Alanine Biosynthesis in *Methanocaldococcus jannaschii*. *J. Bacteriol.* 196, 2869-2875.
- Williams, B.B., Van Benschoten, A.H., Cimermancic, P., Donia, M.S., Zimmermann, M., Taketani, M., Ishihara, A., Kashyap, P.C., Fraser, J.S., Fischbach, M.A., 2014. Discovery and characterization of gut microbiota decarboxylases that can produce the neurotransmitter tryptamine. *Cell host & microbe* 16, 495-503.
- Winn, M.D., Ballard, C.C., Cowtan, K.D., Dodson, E.J., Emsley, P., Evans, P.R., Keegan, R.M., Krissinel, E.B., Leslie, A.G., McCoy, A., McNicholas, S.J., Murshudov, G.N., Pannu, N.S., Potterton, E.A., Powell, H.R., Read, R.J., Vagin, A., Wilson, K.S., 2011. Overview of the CCP4 suite and current developments. *Acta Crystallogr D Biol Crystallogr* 67, 235-242.
- Zhu, H., Xu, G., Zhang, K., Kong, X., Han, R., Zhou, J., Ni, Y., 2016. Crystal structure of tyrosine decarboxylase and identification of key residues involved in conformational swing and substrate binding. *Sci. Rep.* 6, 27779.